materials by using finite element analysis. It was found that wall roughness on contact with the fluid is important for yield strengths, especially in low magnetic fields (9,10). Size and size distribution of the suspended particles also affect the change in properties of the MR fluid when placed in a magnetic field (11,12). The combined effect of magnetic and electric fields on magnetoelectrorheological materials has also been explored (13). Tang and Conrad conducted a series of systematic experiments to characterize the rheology of MR fluids from technological and scientific viewpoints (14).

APPLICATIONS

Because the state of MR materials can be controlled by the strength of an applied magnetic field, it is useful in applications where variable performance is desired. Many smart systems and structures would benefit from the change in viscosity or other material properties of MR materials. Beginning with the commercialization of MR fluid rotary brakes for use in aerobic exercise equipment in 1995, application of magnetorheological material technology in real-world systems has grown steadily. The past few years have witnessed a blossoming commercialization of MR fluid technology. MR fluid technology has been embraced by a number of manufacturers for inclusion in a diverse spectrum of products that are now commercially available (15):

- linear MR dampers for real-time active vibrational control systems in heavy duty trucks
- linear and rotary brakes for low-cost, accurate, positional and velocity control of pneumatic actuator systems
- rotary brakes to provide tactile force-feedback in steer-by-wire systems
- linear dampers for real-time gait control in advanced prosthetic devices
- adjustable shock absorbers for NASCAR oval and dirt track racing

Other applications that are near commercialization include

- low-cost MR sponge dampers for washing machines (16,17)
- very large MR fluid dampers for seismic damage mitigation in civil engineering structures (17)
- large MR fluid dampers to control wind-induced vibrations in cable-stayed bridges (18)
- real-time controlled shock absorbers and struts for domestic automobiles

MR materials are also being considered for use in compliant mechanism design to change the compliance of flexible members. This behavior can be modified as a function of time resulting in a variably compliant mechanism (19). More applications are being considered and it is likely that, as MR materials continue to improve, many more applications will be forthcoming.

BIBLIOGRAPHY

1. J. Rabinow, *AIEE Trans*. **67**: 1308–1315 (1948).
2. Magnetic Fluid Torque and Force Transmitting Device. U.S. Pat. 2,575,360, 1951, J. Rabinow.
3. A. Duff, *Phys. Rev*. **4**: 23 (1986).
4. W.M. Winslow, *J. Appl. Phys.* **20**: 1137–1140 (1949).
5. http://www.mrfluid.com, 2001.
6. D.J Klingenberg, *Sci. Am*. pp. 112–113 (Oct. 1993).
7. J.M. Ginder and L.C. Davis, *Appl. Phys. Lett*. **65**: 3410–3412 (1994).
8. K.D. Weiss, T.G. Duclos, J.D. Carlson, M.J. Chrzan, and A.J. Margida, 1993 Int. Off-Highway & Powerplant Congr. Exposition, SAE Technical Paper Series, #932451.
9. T. Miyamoto and M. Ota, *Appl. Phys. Lett.* **64**: 1165–1167 (1994).
10. E. Lemarie, and G. Bossis, *J. Phys. D* **24**: 1473–1477 (1991).
11. E. Lemaire, A. Mennier, G. Bossis, J. Liu, D. Felt, P. Bashtovioi., and N. Matousseritch, *J. Rheol*. **39**: 1011–1020 (1995).
12. Method and Magnetorheological Fluid Formulations for Increasing the Output of a Magnetorheological Fluid, US Pat. 6,027,664, (2000), and US Pat. 5,900,184, (1999), K.D. Weiss, J.D. Carlson, and D.A. Nixon.
13. K. Koyama, *Proc. 5th Int. Conf. Electro-Rheological, Magneto-Rheological Suspensions Associated Technol.*, Sheffield, U.K., July 1995.
14. X. Tang and H. Conrad, *J. Rheol.***40**(6): 1167–1178 (1996).
15. J.D. Carlson and J.L. Sproston, *Proc. 7th Int. Conf. New Actuators,* Messe Bremen, Bremen, (2000), pp. 126–130.
16. J.D. Carlson, *Mach. Design*, pp. 73–76, Feb. 22, (2001).
17. J.D. Carlson, *Motion Control*, pp. 25–28, March 2001.
18. B.F Spencer, Jr., G. Yang, J.D. Carlson, and M.K Sain, *Proc. 2nd World Conf. Struct. Control*, Kyoto, Japan, 1998.
19. A.J.M. Henrie and L.L Howell, *Proc. 43rd Int. SAMPE* Symp./Exhibition, Irvine, CA, 1998.

MAGNETOSTRICTIVE MATERIALS

MARCELO J. DAPINO
Ohio State University
Columbus, OH

INTRODUCTION

Magnetostrictive materials are a class of smart materials that can convert energy between the magnetic and elastic states. For this reason, magnetostrictive materials and devices based on these materials are often referred to as *transducers*. Due to the bidirectional nature of this energy exchange, magnetostrictive materials can be employed for both actuation and sensing. Alloys based on the transition metals iron, nickel, and cobalt in combination with certain rare-earth elements are currently employed in actuator and sensor systems in a broad range of industrial,

biomedical, and defense applications. Because magnetostriction is an inherent property of ferromagnetic materials, it does not degrade over time as do some poled piezoelectric substances. In addition, newer magnetostrictive materials provide strains, forces, energy densities, and coupling coefficients that compete favorably with more established technologies such as those based on piezoelectricity. As evidenced by the ever-increasing number of patented magnetostrictive systems, transducer designers are finding new opportunities to employ magnetostrictive materials in a wide variety of applications ranging from stand-alone transducers to complex smart structure systems.

A number of design and modeling issues, however, complicate the implementation of magnetostrictive materials in certain applications in which other smart material technologies are currently favored. For instance, due to the required solenoid and related magnetic circuit components, magnetostrictive transducers are usually larger and bulkier than their piezoelectric or electrostrictive counterparts. Hence, they are employed primarily in applications that require high strains and forces but where weight is not an issue. One additional consideration is that the most technologically advanced magnetostrictive materials are costly to manufacture. Advanced crystalline materials are manufactured by employing sophisticated crystal growth techniques that produce directional solidification along the drive axis of the transducer material. The manufacturing process also includes precision machining of laminations, final diameters, and parallel ends of cut-to-length drivers, as well as thorough quality assurance and performance evaluation throughout the process. These technological and cost-related problems have been mitigated to some extent through the advent of new manufacturing techniques that have enabled more capable magnetostrictive materials in various forms, including amorphous or crystalline thin films, magnetostrictive particle-aligned polymer matrix composite structures, and sintered powder compacts suitable for mass production of small irregular shapes. From the perspective of modeling and control, magnetostrictive materials exhibit nonlinear effects and hysteretic phenomena to a degree which other smart materials, for instance electrostrictive compounds, do not. These effects are particularly exacerbated at the moderate to high drive level regimes in which magnetostrictive materials are most attractive. These issues have been addressed through recent modeling techniques, and as new applications are developed, model accuracy and completeness will almost surely follow.

The term magnetostriction is a synonym for magnetically induced strain, and it refers to the change in physical dimensions exhibited by most magnetic materials when their magnetization changes. Magnetization, defined as the volume density of atomic magnetic moments, changes as a result of the reorientation of magnetic moments in a material. This reorientation can be brought about by applying either magnetic fields, heat or stresses. The linear magnetostriction $\Delta L/L$ that results from applying a longitudinal magnetic field on a sample of length L, illustrated in Fig. 1, is the most commonly employed attribute of the magnetostrictive principle in actuator applications. Though most ferromagnetic materials exhibit linear magnetostriction, only a small number of compounds that contain rare-earth elements provide "giant" magnetostrictions in excess of 1000×10^{-6}. These large magnetostrictions are a direct consequence of the strong magnetomechanical coupling that arises from the dependence of magnetic moment orientation on interatomic spacing. When a magnetic field is applied to a magnetostrictive material, the magnetic moments rotate to the direction of the field and produce deformations in the crystal lattice and strains in the bulk material. Referring again to Fig. 1 which pertains to a material that has positive magnetostriction, note

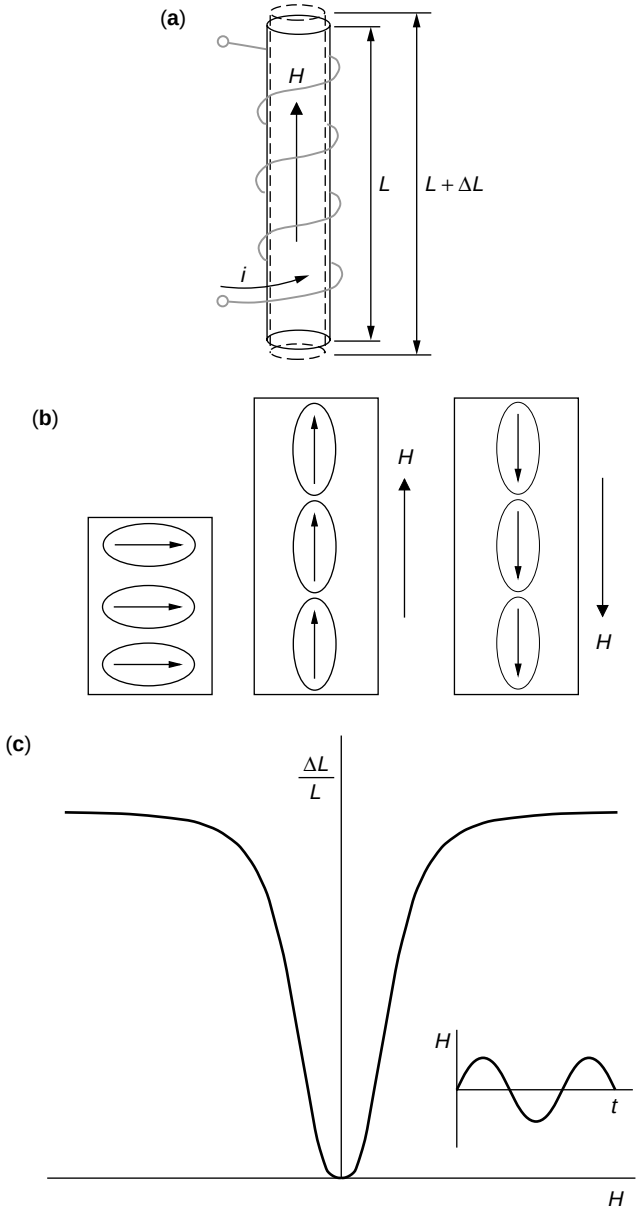

Figure 1. Joule magnetostriction produced by a magnetic field H. (a) H is approximately proportional to the current i that passes through the solenoid when a voltage is applied to it. (b) The rotation of magnetic dipoles changes the length of the sample, and (c) curve $\Delta L/L$ vs. H obtained by varying the field sinusoidally.

that the sample elongates irrespective of the direction of rotation of the magnetic moments. A symmetrical magnetostriction curve is obtained when the field is cycled, as depicted in Fig. 1b,c. If stress is applied instead, the material deformations lead to magnetic moment reorientation and a subsequent change in the magnetization M. This magnetization change can be detected through the voltage induced in a sensing solenoid wrapped around the sample, which provides a mechanism for sensing. In applications, either one sensing solenoid or a plurality of them arranged along the length of the driver can be placed inside of the driving coil. Alternatively, it is possible to employ only one solenoid to drive the magnetostrictive material and sense its magnetization changes. This configuration exhibits the major disadvantage that additional signal processing hardware is required to extract the sensing voltage from the driving signal.

This article provides an overview of magnetostrictive materials in the next section, followed by a description of the physical origin of magnetostriction and a discussion of material behavior. The subsequent section is devoted to linear magnetostriction, and other magnetostrictive effects are discussed in the following section. Finally, a discussion of current transducer designs and modeling techniques is presented.

MATERIALS OVERVIEW

The study of magnetostriction began in 1842 when James P. Joule first observed that a sample of iron changes in length when magnetized by a magnetic field. Subsequent work using other materials such as nickel, cobalt, and their alloys led to numerous applications, including telephone receivers, hydrophones, scanning sonar, fog horns, oscillators, and torque sensors. During World War II, sonar transducer were driven primarily by nickel, which exhibits saturation magnetostrictions of about 50×10^{-6}. A breakthrough in magnetostrictive materials occurred in 1963 when the largest-known magnetostrictions in the rare-earth elements terbium and dysprosium were discovered. The strains in these elements are of the order of $10{,}000\times10^{-6}$, or three orders of magnitude larger than those of nickel, but they are achieved exclusively at cryogenic temperatures. The temperature limitation and the fact that the field of piezoelectricity was gaining technical maturity hindered the development of magnetostrictive materials and led, in the early 1970s, to a search for a new class of transducer materials capable of high room temperature strains. Highly magnetostrictive rare earths (R), principally samarium (Sm), terbium (Tb), and dysprosium (Dy), were combined with the magnetic transition metals nickel, cobalt, and iron by direct compound synthesis and by rapid sputtering into amorphous alloys. In contrast to the normal Curie temperature behavior of the R–Ni and R–Co compounds, R–Fe compounds exhibit an *increase* in the Curie temperature as rare-earth concentration increases. Consequently, huge room temperature magnetostrictions up to $3{,}000\times10^{-6}$ were achieved, particularly in the $TbFe_2$ compound. However, because the magnetostriction originates in the strain dependence of magnetic anisotropy, the large magnetostriction in these compounds is obtained at the expense of large anisotropies. This poses a technological limitation since impractically large fields of more than 2 MA/m are needed to bring these compounds to technical saturation.

Partial substitution of dysprosium for terbium in the $TbFe_2$ system resulted in improved magnetostriction and anisotropy properties. The resulting pseudobinary compound $Tb_{0.3}Dy_{0.7}Fe_{1.9-1.95}$ has been available commercially since the 1980s under the name Terfenol-D (Ter = terbium, Fe = iron, N = Naval, O = Ordnance, L = Laboratory, D = dysprosium). The highest room temperature magnetostriction for Terfenol-D is $1{,}600\times10^{-6}$ at a moderate saturation field of 0.16 MA/m, but even larger magnetostrictions up to $3{,}600\times10^{-6}$ are possible when the material is employed in transducers driven at resonance. The utility of Terfenol-D as a rugged, high-power transducer driver has been increasingly recognized in recent years. At present, Terfenol-D is used in active noise and vibration control systems; low-frequency underwater communications (sonar); linear and rotational motors; ultrasonic cleaning; machining and welding; micropositioning; and detecting motion, force, and magnetic fields. Terfenol-D is currently available in a variety of forms, including monolithic rods (1,2), particle-aligned polymer matrix composites (3–5), and thin films (6,7). Because of the large magnetostrictive anisotropy and strong magnetoelasticity, Terfenol-D and other pseudobinary rare-earth–iron compounds can be synthesized to exhibit a broad range of properties (8).

A second new magnetostrictive material based on amorphous metal was introduced in 1978, produced by rapid cooling of iron, nickel, and cobalt alloys together with one or more of the elements silicon, boron, and phosphorus. These alloys are known commercially as Metglas (metallic glass) and are commonly produced in thin-ribbon geometries. Because of the extremely high coupling coefficients ($k > 0.92$), Metglas is a prime candidate for sensing applications in which a mechanical motion is converted into an electrical current or voltage (2).

The latest materials science research on magnetostrictive materials includes the development of new compounds to minimize magnetic anisotropy and hysteresis and new manufacturing techniques to produce Terfenol-D thin films efficiently (9). Substantial advances have been achieved in the quaternary compounds Terfenol-DH, which are produced by substituting holmium for terbium and dysprosium (10). In addition, new manufacturing techniques are enabling the production of multilayered driver rods which will lead to reduced dynamic losses, thus facilitating operation over a broad frequency spectrum into the megahertz range. Ferromagnetic shape-memory alloys are another class of smart materials which hold much promise due to the large strains that they can provide. The nickel–titanium alloy commercially known as Nitinol features large recoverable strains of the order of $60{,}000\times10^{-6}$, but it suffers from inferior dynamic response. The possibility of combining the desirable aspects of shape memory with magnetostriction through actuating an SMA in a magnetic

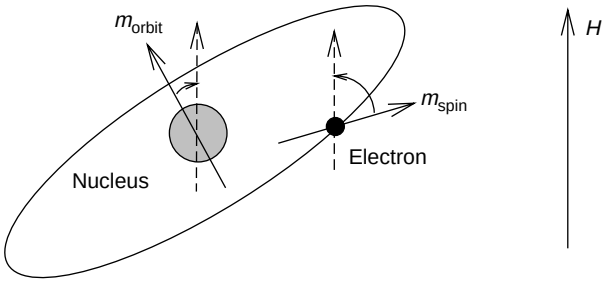

Figure 2. In highly magnetostrictive materials, the spin moment m_{spin} and orbital moment m_{orbit} are strongly coupled. When the spin moment rotates to align with the external field H, the orbital moment rotates along with it and produces considerable lattice deformation.

field is currently being investigated. Promising candidate materials are the Ni_2MnGa system and the Fe-based Invars, which exhibit, in principle, the desired characteristics. Further details on the Ni–Mn–Ga alloys can be found in (11,12).

PHYSICAL ORIGIN OF MAGNETOSTRICTION

Magnetic coupling within atoms can be of two forms, spin–spin and spin–orbit interactions. In ferromagnetic materials, the spin–spin coupling that keeps neighboring spins parallel or antiparallel to one another within domains can be very strong. However, this exchange energy is isotropic because it depends only on the angle between adjacent spins, not on the direction of the spins relative to the crystal lattice.

Magnetostriction is due mainly to spin–orbit coupling, which refers to a kind of interaction between the spin and orbital motion of each electron. This type of coupling is also responsible for crystal anisotropy. Referring to Fig. 2, when a magnetic field is applied and an electron spin tries to align with it, the orbit of that electron also tends to be reoriented. But because the orbit is strongly coupled to the crystal lattice, the orbit resists the rotation of the spin axis. Thus, the energy required to rotate the spin system of a domain away from the preferred orientations is the energy required to overcome spin–orbit coupling. Spin–orbit coupling is weak in most ferromagnetic materials, as evidenced by the fact that a moderate field of a few thousand kiloamperes per meter suffices to rotate the spins. Spin–orbit coupling in rare-earth metals is much stronger by about an order of magnitude. When a magnetic field rotates the spins, the orbital moments rotate, and considerable distortion, and hence magnetostriction, results (13).

MATERIAL BEHAVIOR

Magnetic Anisotropy

Magnetic anisotropy refers to the dependence of magnetic properties on the direction in which they are measured. It can be of several kinds, including crystal, stress, shape, and exchange anisotropy. Of these, however, only crystal anisotropy is intrinsic to the material, whereas the other types are externally induced.

In crystalline materials, the magnetic moments do not rotate freely in response to applied fields, but rather they tend to point in preferred crystallographic directions. This phenomenon is called magnetocrystalline (or crystal) anisotropy, and the associated anisotropy energy is that required to rotate the magnetic moments away from their preferred direction. Crystal anisotropy energy and linear magnetostriction are closely related. If anisotropy is independent of the state of strain, there will be no linear magnetostriction (14). In rare-earth elements, for instance, large strains are a direct consequence of the huge strain dependence of magnetic anisotropy (8). Under the action of a magnetic field, measurable strains result from the deformations that the crystal lattice undergoes to minimize the energy state of the material.

When a sinusoidal magnetic field is applied to a material that has sufficiently large anisotropy, the resulting magnetization curve is not smooth due to the presence of magnetic moment "jumping." For example, Fig. 3a,b shows the magnetization and magnetostriction of the alloy $Tb_{0.67}Dy_{0.33}$, which has substantial magnetic anisotropy. The discontinuity in both curves near a field value of 40 kA/m occurs because the magnetic moments abruptly enter or leave low energy directions. Elements that have

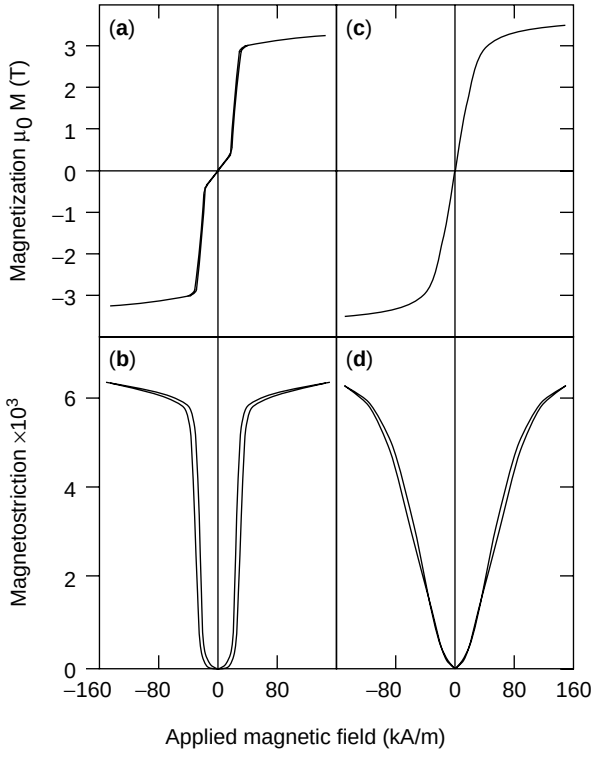

Figure 3. (a,b) Magnetization and magnetostriction jumps in $Tb_{0.67}Dy_{0.33}$, a material that has large anisotropy. (c), (d) The same measurements are much smoother in a material that has near zero anisotropy such as $Tb_{0.6}Dy_{0.4}$ (36).

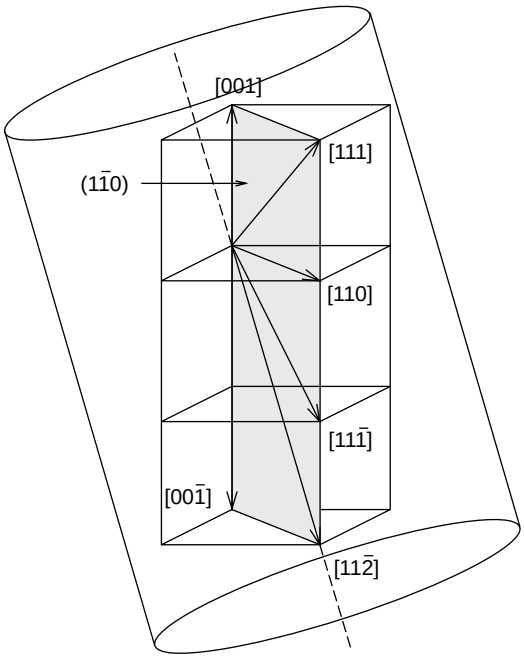

Figure 4. Crystallographic orientations in monolithic Terfenol-D. The square brackets represent the indexes of particular directions such as the edges of a cube: [100], [010], [001], [$\bar{1}$00], [0$\bar{1}$0], and [00$\bar{1}$], in which $\bar{1}$ denotes -1. The entire set of directions is designated by any one direction in angular brackets, for instance, <100>. Finally, planes of a form are designated by rounded brackets, such as the six faces of a cube: (100), (010), (001), ($\bar{1}$00), (0$\bar{1}$0), and (00$\bar{1}$).

opposite anisotropies are often alloyed together to reduce the jumping and associated nonlinearities in material behavior. Such a material is shown in Fig. 3c,d. In this case, the same system but in a different composition ($Tb_{0.6}Dy_{0.4}$) exhibits a much smoother response to the applied field.

Accurate models for crystal anisotropy and its relationship to the magnetization process exist for simple cases of cubic and hexagonal crystals (15,16), but models of complex crystal structures often rely on simplifying assumptions that reduce the problem to the simpler cases. For instance, it is often useful to assume operating regimes in which stress anisotropy dominates crystal anisotropy, thus enabling the modeling of highly complex cases such as that of Terfenol-D whose crystals are grown in dendritic twin sheets oriented in the [11$\bar{2}$] direction, as shown in Fig. 4 and discussed in (1). Terfenol-D has a large and positive magnetostrictive coefficient of $\lambda_{111} = +1{,}600 \times 10^{-6}$, so a compressive stress applied along the (11$\bar{2}$) direction produces a significant decrease in the internal energy of the crystal at *right angles* to the applied stress. On the other hand, although the anisotropy coefficient of Terfenol-D varies significantly, depending on temperature and stoichiometry ($K_1 = -4$ to -50 kJ/m^3 [3,17]), it is sufficiently large to resist such energy changes by favoring alignment in the <111> directions. Then, it is inferred that a sufficiently large compressive stress will raise the elastic energy above that of the crystal anisotropy, shifting the preferred orientation of domains to the <111> magnetic easy axes that are perpendicular to the [11$\bar{2}$] direction. Under such compressive stress, the population density in these two orientations increases, and a magnetic field applied in the [11$\bar{2}$] direction produces nearly isotropic 90° rotations because the energy wells of crystal anisotropy have been effectively removed from the path of the rotations. In addition, under compression, as large populations of magnetic moments align normally to the stress direction, the demagnetized length decreases to a minimum, and the saturation magnetostrictive potential increases to a maximum. The 90° rotations subsequently provide the maximum possible magnetostrictions. To summarize, in materials that have positive magnetostrictions like Terfenol-D, the stress anisotropy generated by compression effectively improves the magnetoelastic state that leads to enhanced magnetostrictions. The manner in which this is implemented in transducer applications is discussed later. In nickel, which has a negative magnetostrictive coefficient, the effect is reversed, and enhanced magnetoelasticity is obtained from tensile stresses. Further details regarding crystal anisotropy can be found in (18–20).

Domain Processes and Hysteresis

The changes in magnetization that result from an applied magnetic field can be either reversible or irreversible. Reversible changes in magnetization are energetically conservative and occur for small field increments in which the material can return to the original magnetic state upon removing the field. Irreversible magnetizations are dissipative because external restoring forces are needed to return the magnetism to its original state, for example, when large fields are applied. In applications, both types of mechanisms contribute to the magnetization process. Magnetization, either reversible or irreversible, can be explained by considering two related mechanisms: the rotation of magnetic moments and the movement of domain walls. The presence of domain walls lies in the domain structure characteristic of ferromagnetic materials below their magnetic phase transition temperature or Curie temperature, T_c (see Table 1 for values of T_c for several magnetostrictive materials). When a ferromagnetic material is cooled below its Curie temperature, the magnetic moments become ordered across volumes, called domains, that contain large numbers of atoms. The domain structure can be observed under a microscope, and it typically consists of 10^{12}–10^{15} atoms per domain. The transition regions between neighboring domains are called domain walls. All of the moments of each domain are aligned parallel, producing a spontaneous magnetization M_s, but without a field, the direction of M_s varies from domain to domain, so that the bulk magnetization in the material averages zero. This is illustrated by the randomly oriented regions of Fig. 5a.

When a small magnetic field H is applied, as depicted in Fig. 5b, domains oriented favorably to the field grow at the expense of the remaining domains, and the main magnetization mechanism is domain wall motion. As the field is increased (see Fig. 5c), entire domains rotate to align

Table 1. Magnetoelastic Properties of Some Magnetostrictive Materials

Material	$\frac{3}{2}\lambda_s(\times 10^{-6})$	ρ (g/cm^3)	B_s (T)	T_c(°C)	E (GPa)	k
Fe	–14 (8)	7.88 (14)	2.15 (14)	770 (14)	285 (14)	
Ni	–50 (14)	8.9 (14)	0.61 (14)	358 (14)	210 (1)	0.31 (8)
Co	–93 (14)	8.9 (14)	1.79 (14)	1120 (14)	210 (1)	
50% Co–50% Fe	87 (2)	8.25 (8)	2.45 (76)	500 (14)		0.35 (8)
50% Ni–50% Fe	19 (2)		1.60 (76)	500 (14)		
$TbFe_2$	2630 (8)	9.1 (14)	1.1 (2)	423 (8)		0.35 (8)
Tb	3000 (−196°C) (36)	8.33 (14)		–48 (13)	55.7 (1)	
Dy	6000 (−196°C) (36)	8.56 (14)		–184 (1)	61.4 (1)	
Terfenol-D	1620 (8)	9.25	1.0	380 (76)	110 (77)	0.77 (78)
$Tb_{0.6}Dy_{0.4}$	6000 (−196°C) (36)					
Metglas 2605SC	60 (36)	7.32 (2)	1.65 (76)	370 (2)	25–200 (2)	0.92 (1)

[a]Unless otherwise specified, all measurements were performed at room temperature.

with the easy [11$\bar{1}$] axis. This produces a burst region in the magnetization versus field (M–H) and strain versus field (ε–H) curves by virtue of which small field changes produce large magnetization or strain changes. In the final stage shown in Fig. 5d, the material acts as a single domain as magnetic moments rotate coherently from the easy axis to the direction of the field. This produces saturation of the magnetization. Typical magnetization and strain loops shown in Fig. 6 illustrate the burst region and saturation effects. From a design perspective, magnetic biasing described later is used to center operation in the burst region for optimum performance.

For low magnetic field levels, partial excursions in the M–H or ε–H curve are observed that are approximately linear. However, hysteresis is always present, particularly when the materials are employed at high field levels such as those of Fig. 6. The hysteresis can be attributed to the irreversible impediment to domain motion by pinning sites, such as when domain walls move across twin boundaries in Terfenol-D. Modeling hysteresis and nonlinear behavior is currently a focal point in designing and controlling magnetostrictive materials. Extensive details on the topic of ferromagnetic hysteresis can be found in (14,21,22).

Material Properties

Strains are generated by magnetostrictive materials when magnetic moments rotate to align with an applied field. This phenomenon is governed by an energy transduction process known as magnetomechanical coupling that is intrinsically bidirectional and that facilitates both actuating and sensing mechanisms in a material. From a design

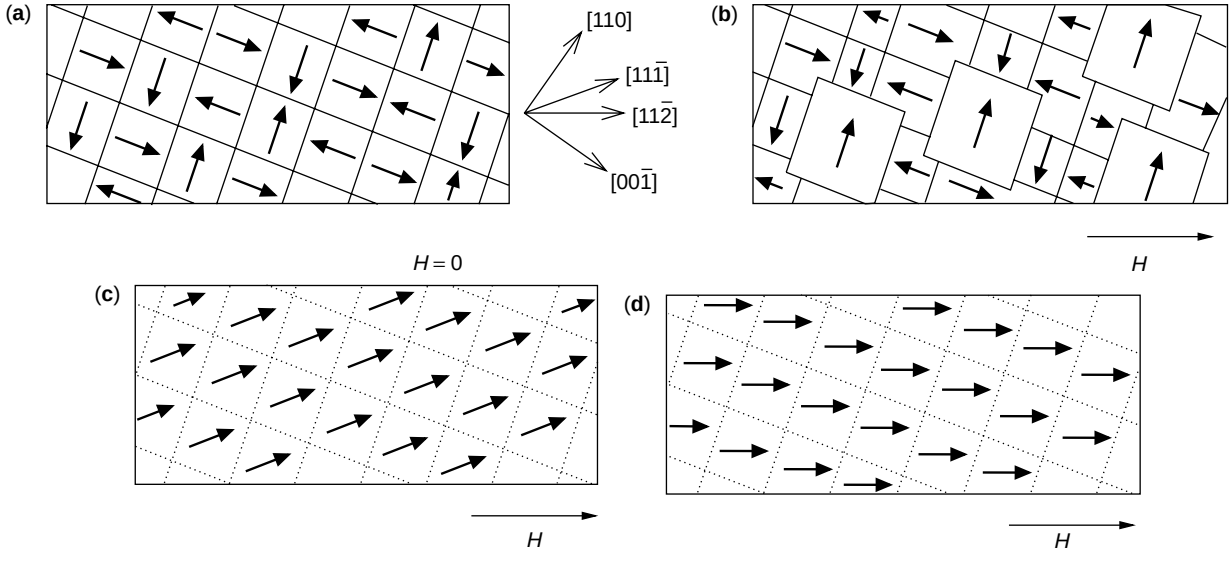

Figure 5. Domain processes in the (1$\bar{1}$0) plane of single crystal Terfenol-D under the application of a field H along the [11$\bar{2}$] axis: (a) demagnetized specimen, (b) partial magnetization by domain-wall movement, (c) from partial magnetization to the knee of the magnetization curve by irreversible domain magnetization rotation into the [11$\bar{1}$] axis, and (d) from the knee of the magnetization curve to technical saturation by reversible (coherent) rotation to the [11$\bar{2}$] axis (21).

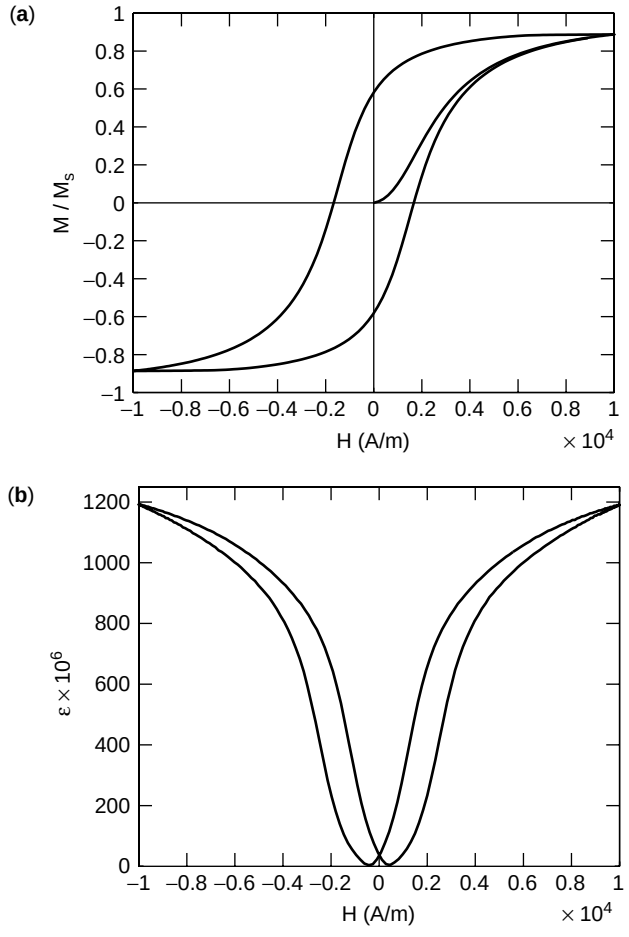

Figure 6. Relative magnetization M/M_s and total strain ε as a function of magnetic field H in a magnetostrictive material.

standpoint, the linear coupling coefficient k that quantifies the conversion efficiency between mechanical and elastic energies must be close to unity. Significant magnetic moment rotation occurs only when a domain structure is present, that is to say, in the ferromagnetic state below the Curie temperature T_c. Hence, the material must be designed so that its Curie temperature is well above the operating temperature range. In smart structure systems, large forces are often involved that the magnetostrictive material must support. The stiffness of the material is quantified by the elastic modulus E. The material must have a large value of E to support large forces. Finally, the magnetostrictive material must feature a large saturation magnetization M_s (or, equivalently, a large saturation induction B_s), and the magnetic anisotropy must be small.

Shown in Table 1 is a list of nominal properties for several magnetostrictive materials of interest. Note that the magnetomechanical coupling responsible for diverse material properties is a highly complex function that depends on quantities such as magnetic field, stress, temperature, and frequency. These quantities are collectively known as "operating conditions" and typically vary during device operation. It has been demonstrated that small variations in operating conditions often produce large changes in material properties (23). Efficient transducer design requires accurately assessing how material properties behave under varying operating conditions.

LINEAR MAGNETOSTRICTION

Linear or Joule magnetostriction pertains to the strain produced in the field direction and is the most commonly used magnetostrictive effect. Because linear magnetostriction occurs at constant volume, there must be a transverse strain of sign opposite to that of the linear magnetostriction,

$$\lambda_\perp = -\frac{\lambda}{2}.$$

Isotropic Spontaneous Magnetostriction

It was mentioned earlier that when a ferromagnetic material is cooled through its Curie temperature, a transition from paramagnetism to ferromagnetism takes place, and magnetic moments become ordered giving rise to spontaneous magnetization M_s within domains. This process is also accompanied by a strain which is known as *spontaneous* magnetostriction λ_0. It is possible to derive a useful relationship between λ_0 and *saturation* magnetostriction λ_s. To that end, we consider an isotropic material in the disordered state above T_c, which is therefore modeled by spherical volumes, as shown in Fig. 7a. As the material is cooled below T_c, spontaneous magnetization M_s is generated within magnetic domains along with the corresponding spontaneous magnetostriction λ_0. The domains are represented in Fig. 7b by ellipsoids that have spontaneous strain e. Because the material is isotropic, the magnetic domains are oriented randomly; each bears an angle θ with respect to the direction of measurement. Net magnetization is consequently zero, and the length in the

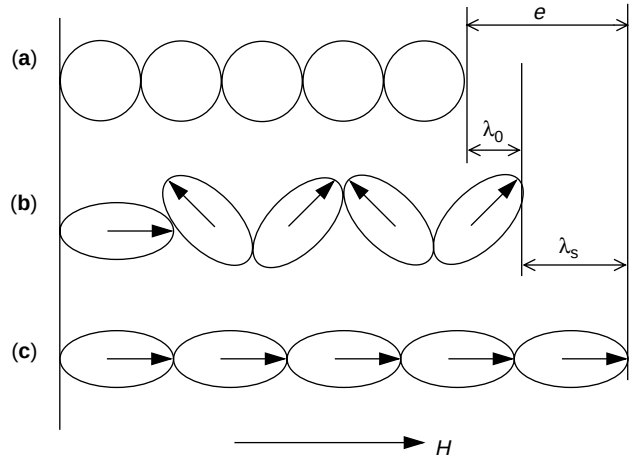

Figure 7. Schematic diagram illustrating the magnetostriction of a ferromagnetic material: (a) paramagnetic state above T_c; (b) after it has been cooled through T_c; and (c) after it has been brought to saturation by a field H.

direction of interest is given by (13)

$$e(\theta) = e\,\cos^2\theta. \tag{1}$$

Then, the average domain deformation at the onset of spontaneous magnetostriction can be obtained by integration in all possible directions,

$$\lambda_0 = \int_{-\pi/2}^{\pi/2} e\,\cos^2\theta\,\sin\theta\,d\theta = \frac{e}{3}.$$

Spontaneous magnetostriction λ_0 is homogeneous in all directions, so that the material has changed its dimensions but not its shape. When a magnetic field is applied, the domains rotate and become aligned either parallel to the field or perpendicular to it, depending on whether the material exhibits positive or negative magnetostriction. Assuming positive magnetostriction, the domains will rotate into the field direction, as depicted in Fig. 7c. Near saturation, the material will be a single domain, and the total strain will be e. Then, the total available saturation magnetostriction is given by the difference between e and λ_0,

$$\lambda_s = e - \lambda_0 = \frac{2}{3}e = 2\lambda_0. \tag{2}$$

This expression provides a method of measuring the spontaneous strain λ_0 by measuring λ_s. Methods to determine λ_s are discussed next.

Saturation Magnetostriction

Assuming again for simplicity that the medium is isotropic, saturation magnetostriction at an angle θ to the direction of the field is given by (13)

$$\lambda_s(\theta) = \frac{3}{2}\lambda_s\left(\cos^2\theta - \frac{1}{3}\right), \tag{3}$$

where $\lambda_s(\theta)$ is the saturation magnetostriction at an angle θ to the field and λ_s is the saturation magnetostriction along the direction of magnetization.

The saturation magnetostriction is then calculated from the difference between the maximum magnetostriction when the field is parallel to a given direction ($\lambda_{s\parallel}$) and that when the field is perpendicular to the given direction ($\lambda_{s\perp}$). Substituting $\theta = 0^\circ$ and $\theta = 90^\circ$ in Eq. (3) gives

$$\lambda_{s\parallel} - \lambda_{s\perp} = \lambda_s + \frac{1}{2}\lambda_s = \frac{3}{2}\lambda_s, \tag{4}$$

which defines λ_s independently of the demagnetized state.

Magnetostriction data from Clark (8) taken from polycrystalline $Tb_xDy_{1-x}Fe_y$ samples are reproduced in Fig. 8. The data points correspond to $\lambda_{s\parallel} - \lambda_{s\perp}$ at room temperature and field values of $H = 10$ kOe (0.8 MA/m) and $H = 25$ kOe (2 MA/m). Near $x = 0.3$, the magnetostrictive curve shows a peak in accordance with the near zero magnetic anisotropy observed at this composition. From the magnetostrictive value at the peak, about 1600×10^{-6},

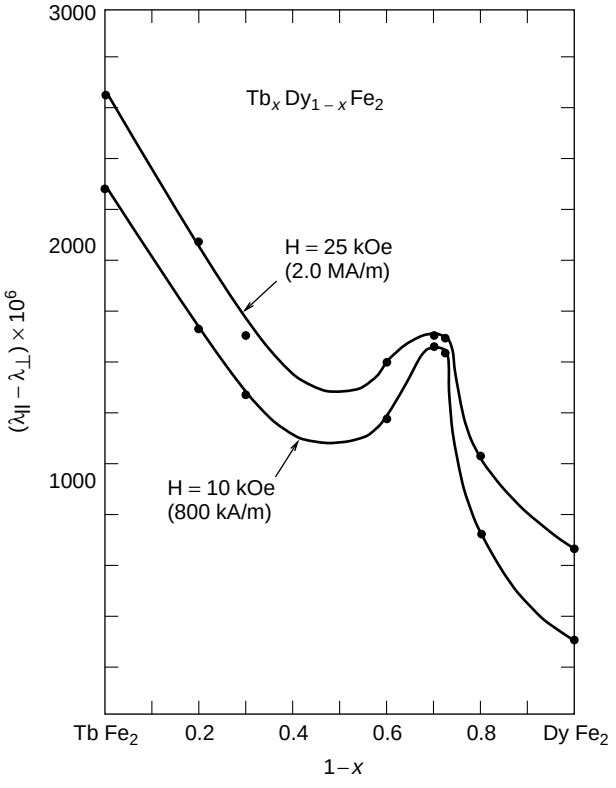

Figure 8. Magnetostriction of polycrystalline $Tb_xDy_{1-x}Fe_2$ at room temperature (8).

Eq. (4) gives $\lambda_s = 1000 \times 10^{-6}$ which is a widely employed value for the saturation magnetostriction of Terfenol-D.

Anisotropy is present to some degree in all magnetic materials, and therefore, the saturation magnetostriction needs to be defined relative to the axis along which the magnetization lies. One exception is nickel, whose magnetostriction is almost isotropic (see Table 2). Recognizing that there are two independent magnetostriction constants λ_{100} and λ_{111} for cubic materials, the saturation magnetostriction, assuming a single crystal, single domain material is given by a generalization of Eq. (3) for isotropic materials:

$$\lambda_s = \frac{3}{2}\lambda_{100}\left(\alpha_1^2\beta_1^2 + \alpha_2^2\beta_2^2 + \alpha_3^2\beta_3^2 - \frac{1}{3}\right) + 3\lambda_{111}(\alpha_1\alpha_2\beta_1\beta_2 + \alpha_2\alpha_3\beta_2\beta_3 + \alpha_3\alpha_1\beta_3\beta_1), \tag{5}$$

where λ_{100} and λ_{111} are the saturation magnetostrictions along the <100> and <111> axes of the crystal. Cosines α_i

Table 2. Magnetostrictive Coefficients of Cubic Crystal Materials

Material	$\lambda_{100}\,(10^{-6})$	$\lambda_{111}\,(10^{-6})$
Nickel	−46	−24
Iron	21	−21
Terfenol-D	90	1600

($i = 1, 2, 3$) define the direction along which the magnetic moments are saturated, and cosines β_i define the direction in which the saturation magnetization is measured. The saturation magnetostriction in the field direction is obtained by using $\alpha_i = \beta_i$ in Eq. (5), which leads to

$$\lambda_s = \lambda_{100} + 3(\lambda_{111} - \lambda_{100})\left(\alpha_1^2\alpha_2^2 + \alpha_2^2\alpha_3^2 + \alpha_3^2\alpha_1^2\right). \quad (6)$$

Note that Eqs. (5) and (6) apply only to single domain materials. In the saturated state, the whole specimen consists of a single domain whose magnetization M_s is aligned parallel to the applied field. However, when a domain structure is present such as in polycrystals, the magnetostriction can be calculated only by averaging the effects, unless the domain structure is known specifically. Note that different domain configurations can give the same bulk magnetization and different magnetostrictions (see Fig. 9). So, assuming that there is no preferred grain orientation, Eq. (6) simplifies further and becomes

$$\overline{\lambda_s} = \frac{2}{5}\lambda_{100} + \frac{3}{5}\lambda_{111}.$$

Extensive magnetostriction data on the R–Fe_2 compounds can be found in (8), and calculations of λ_s in different crystallographic structures such as cubic, hexagonal, and polycrystalline can be found in (2,13,16,21).

Magnetostriction below Saturation

Although saturation magnetostriction λ_s can be determined by employing the methods previously discussed, magnetostriction between the demagnetized state and saturation is structure sensitive, so general constitutive relationships for magnetostriction are not feasible. However, an explicit solution exists when strains are due primarily to 90° domain rotations. In practice, these rotations occur in (1) a single crystal that has uniaxial anisotropy in which the field is applied in a direction perpendicular to the easy axis or (2) a polycrystalline material in which the magnetic moments have been completely aligned in a direction perpendicular to the applied field, such as Terfenol-D under extreme compression or nickel under tension. The latter implies that perpendicular stress energy is sufficient to dominate crystal anisotropy, as discussed earlier. For that regime, combining Eqs. (1) and Eq. (2) gives

$$\lambda = \frac{3}{2}\lambda_s \cos^2\theta, \quad (7)$$

where θ is the angle between the M_s vectors and the field direction. Recognizing that the bulk magnetization in the field direction is given by $M = M_s \cos\theta$, Eq. (7) becomes

$$\lambda = \frac{3}{2}\lambda_s \left(\frac{M}{M_s}\right)^2, \quad (8)$$

which provides a quadratic relationship between magnetization and magnetostriction. It has been shown that this expression is sufficiently accurate in a broad range of transducer regimes in which high mechanical preloads are employed to optimize transducer performance (24). A generalized version of this equation has been given in (25), and more elaborate models of magnetostrictive hysteresis have been presented in (19,26–28). Additional effects such as stress dependences have been also considered (25,29). Finally, the dependence of the magnetostriction of the R–Fe_2 compounds on temperature has been discussed in (8).

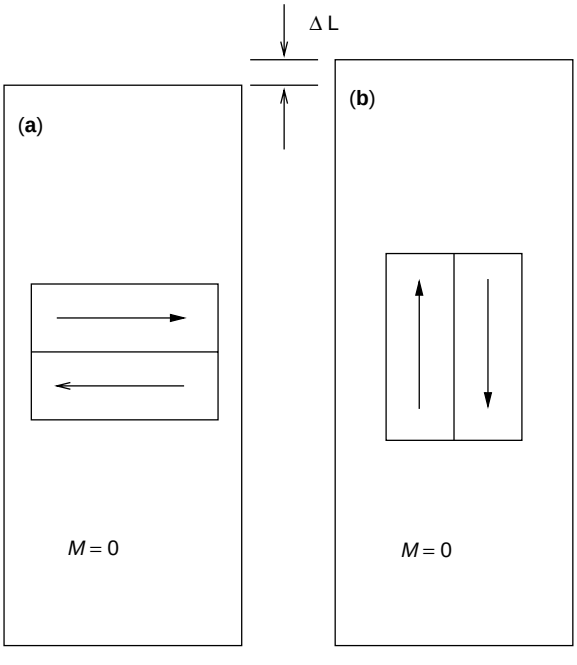

Figure 9. Demagnetized specimen featuring a 180° domain wall in the (a) horizontal or (b) vertical direction. The length of the specimen is different in either case, even though the magnetization is the same.

OTHER MAGNETOSTRICTIVE EFFECTS

Linear magnetostriction is just one of several manifestations of a more general phenomenon, the coupling between the magnetic and elastic states in a material. These effects are briefly discussed following and are summarized in Table 3.

Villari Effect

The Villari effect, also known as the magnetomechanical effect, are the changes in magnetization that a magnetostrictive material undergoes when subjected to an applied uniaxial stress. This effect pertains to the transduction of energy from the elastic to the magnetic state and is inverse of Joule magnetostriction. Furthermore, the Villari effect exhibits many of the attributes of the direct magnetostrictive effect inasmuch as its physical origin also lies in magnetoelastic coupling. The Villari effect has been the object of much study, given its relevance in applications such as nondestructive evaluation and sensing. Extensive theoretical and experimental details can be found in (25). The effect of stress on magnetostrictive materials in particular has been discussed in (30).

Table 3. Magnetostrictive Effects

Direct Effects	Inverse Effects
Joule magnetostriction Change in sample dimensions in the direction of the applied field	**Villari effect** Change in magnetization due to applied stress
ΔE effect Magnetoelastic contribution to magnetocrystalline anisotropy	Magnetically induced changes in elasticity
Wiedemann effect Torque induced by helical anisotropy	**Matteuci effect** Helical anisotropy and emf induced by torque
Magnetovolume effect Volume change due to magnetization (most evident near the Curie temperature)	**Nagaoka–Honda effect** Change in the magnetic state due to a change in volume

ΔE Effect

The elasticity of magnetostrictive materials is composed of two separate but related attributes, the conventional stress–strain elasticity that arises from interatomic forces and the magnetoelastic contribution due to the rotation of magnetic moments and the ensuing strain that occur when a stress is applied. The latter contribution, known as the ΔE effect, is quantified by $\Delta E = (E_s - E_0)/E_0$, where E_0 is the minimum elastic modulus and E_s is the elastic modulus at magnetic saturation. Because the strain produced by magnetic moment rotation adds to the non-magnetic strain [see Eq. (9)], the material becomes softer when the moments are free to rotate. This is illustrated in Fig. 10. Note that the material becomes increasingly stiff as saturation is approached and magnetic moment mobility decreases. The ΔE effect is small in nickel ($\Delta E = 0.06$) but is quite large in Terfenol-D (ΔE up to 5) and certain transverse-field annealed $Fe_{81}B_{13.5}Si_{3.5}C_2$ (Metglas 2605SC) amorphous ribbons ($\Delta E = 10$). The ΔE effect of Terfenol-D can be advantageously employed in tunable vibration absorbers and broadband sonar systems (31).

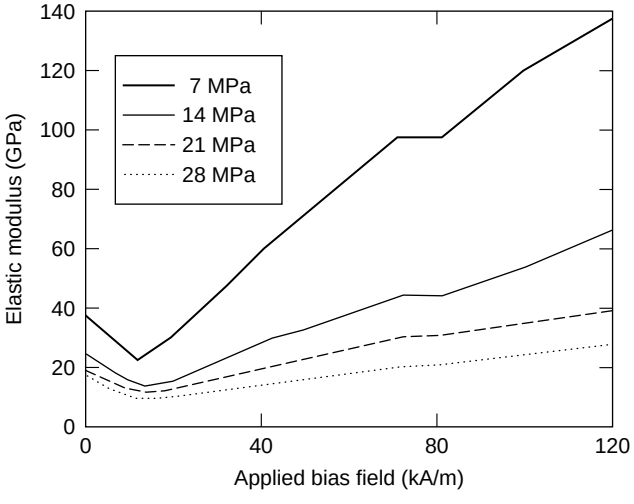

Figure 10. Magnetoelastic modulus of $Tb_{0.3}Dy_{0.7}Fe_2$ under various stresses (79).

Wiedemann Effect

A current-carrying ferromagnetic or amorphous wire produces a circular magnetic field in a plane perpendicular to the wire, and the moments align predominantly in the circumferential direction. When an axial magnetic field is applied, some of the moments align helically and create a helical magnetic field. The twist observed in the wire is called the Wiedemann effect. The inverse Wiedemann effect, known as the Matteuci effect, is the change in axial magnetization of a current-carrying wire when it is twisted. Further details can be found in (2).

Magnetovolume Effect

The volume of a magnetostrictive material remains virtually unchanged during normal operation, but in certain extreme regimes, the volume of the material may change in response to magnetic fields. This anomalous volume change is called the volume magnetostriction or Barret effect. The effect has little applicability in smart structure systems. For instance, the magnetostriction curve of nickel rapidly reaches -35×10^{-6} at only 10 kA/m, but the fractional volume change is only 0.1×10^{-6} in a much larger field of 80 kA/m. In the alloy Invar (36% nickel–64% iron), the fractional volume change at the Curie temperature, which is slightly above room temperature, compensates for the intrinsic thermal expansion and gives a compound that has nearly zero thermal expansion at room temperature. The inverse of the Barret effect, the Nagaoka–Honda effect, is the change in magnetic state caused by a volume change (2,14).

MAGNETOSTRICTIVE TRANSDUCERS

One advantage of magnetostrictive transducers over other types of transducers is that they can be driven by conventional low impedance amplifiers, particularly at frequencies well below resonance; in this case, the low impedance of a magnetostrictive transducer means that driving voltages can be low. This can prove useful in medical applications and in general can greatly simplify amplifier design. Figure 11 shows the measured complex electrical impedance frequency response function $Z_{ee} = V/I$ of a Terfenol-D transducer designed following the generic

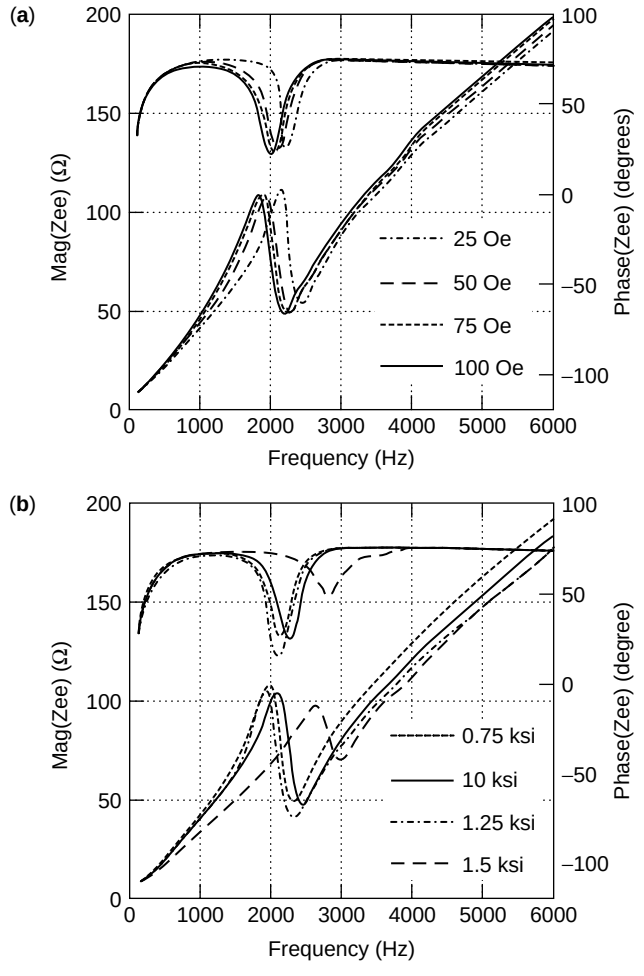

Figure 11. Total electrical impedance Z_{ee} versus frequency, expressed as magnitude and phase: (a) bias condition of 5.2 MPa, 24 kA/m (0.75 ksi, 300 Oe), and varied ac drive levels; (b) constant ac drive level of 8 kA/m (100 Oe) and varied bias conditions (79).

configuration indicated in Fig. 12 (32,33). This transducer consists of a cylindrical magnetostrictive rod, a surrounding copper-wire solenoid, a preload mechanism that consists of a bolt and a spring washer, magnetic couplers, and a barrel-like permanent magnet that provides bias magnetization. Specific design details depend on the particular smart structure application; however, this configuration depicts the basic components needed to extract maximum performance from a magnetostrictive material.

Because magnetostriction is produced by the rotation of magnetic moments, a magnetostrictive transducer driven by an ac magnetic field vibrates at twice the drive frequency, and the motion occurs in only one direction. This is illustrated in Fig. 13, where the solid lines represent the unbiased input and corresponding strain output. The dashed lines demonstrate the performance improvements achieved by applying a magnetic bias. In the biased regime, the frequency of the input is preserved, the output is bidirectional, and the ratio of output per input is substantially larger. To center operation accurately around the

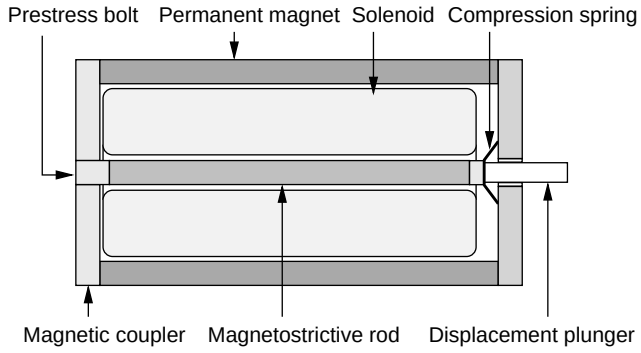

Figure 12. Cross section of a typical magnetostrictive transducer.

desired bias point, a permanent magnet is often employed in combination with a static field generated by passing a dc current through the solenoid. Note that exclusive permanent magnet biasing has the advantage of substantial power savings, but it has the disadvantage of added bulk and weight. Conversely, dc currents produce considerable power losses through ohmic heating but facilitate savings in bulk and weight. Magnetic biasing can be alternatively provided by magnets located in series with the rod or rods; this design is known as a stacked-magnet configuration. The stacked-magnet configuration can improve the magnetomechanical coupling up to 5% for large rods ($L > 20$ cm, $D > 2.5$ cm) compared to the barrel-magnet configuration. However, collateral problems such as saturation effects and resonance frequency shifts are common in stacked-magnet designs. Carefully designed transducers must provide efficient magnetic flux closure within the circuit formed by the rod itself, the couplers, and the permanent magnets.

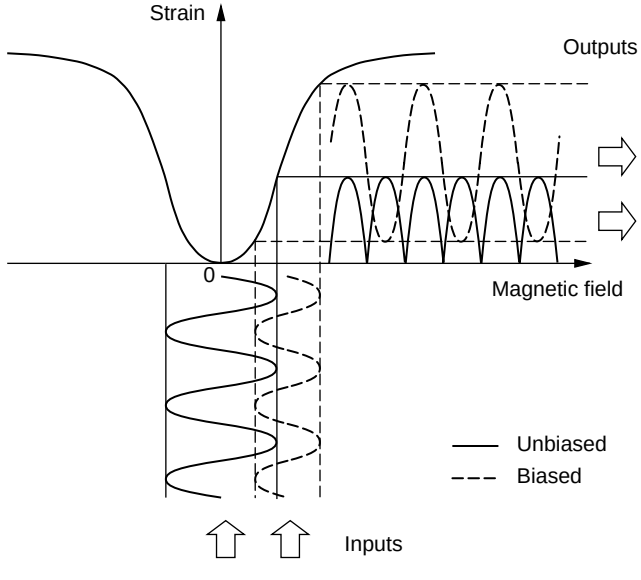

Figure 13. Effect of magnetic bias on the strain produced by a magnetostrictive transducer.

Finally, although modern magnetostrictive materials such as Terfenol-D are manufactured so that their magnetic moments are nearly perpendicular to the rod axis, a static stress (mechanical preload) is nevertheless, required to achieve full alignment of all of the moments. The moments of a mechanically free rod are aligned randomly, and the rod produces only about half of its maximum magnetostriction because the moments initially aligned with the rod axis do not contribute to the magnetostriction. Furthermore, the stress anisotropy generated by the static compression (or tension for materials of negative magnetostriction) enhances the overall magnetoelastic state, as described previously. Note that in designs that employ linear washers for preloading, the stress in the magnetostrictive rod can vary significantly relative to the nominal preload during dynamic transducer operation. By virtue of the magnetomechanical coupling, this can have a profound impact on the performance of the magnetostrictive transducer and driving electronics by affecting the magnetic state and, through it, the electrical regime (see Fig. 11). The effects of mechanical preload and magnetic bias on the performance of a Terfenol-D transducer have been studied in (34). A second reason for employing a mechanical preload is to avoid operating the rod in tension, particularly when driving brittle materials such as Terfenol-D ($\sigma_t = 28$ MPa, $\sigma_c = 700$ MPa) at or near mechanical resonance.

Actuator Applications

The number of actuator applications based on magnetostrictive materials, mainly Terfenol-D, is continuously increasing as a consequence of the high energy density, high force, broad frequency bandwidth, and fast response that these materials provide. Even though the cost of Terfenol-D is high at present, the range of applications is likely to continue increasing as manufacturing techniques are perfected and prices decline. Actuators designed according to the configuration shown in Fig. 12 have been employed in these applications: sonar, chatter control for boring tools, high-precision micropositioning, borehole seismic sources, geological tomography, hydraulic valves for fuel injection systems, deformable mirrors, hydraulic pumps, bone-conduction hearing aids, exoskeletal telemanipulators, self-sensing actuators, degassing in manufacturing processes such as rubber vulcanization, and industrial ultrasonic cleaning. Four main application subgroups of current transducer designs are discussed here: sonar transducers, linear motors, rotational motors, and hybrid smart material transducers. The reader is directed to (1,2) for more complete details.

Sonar Transducers. Efficient sonar transducers must produce high mechanical power at low frequencies and often have the additional constraint that a broad frequency bandwidth or equivalently, a low quality factor Q, must be attained. Although nickel was widely employed in sonar applications during World War II, it has a low magnetomechanical coupling coefficient of $k = 0.30$ which typically demands a high Q to achieve good efficiencies. In contrast, the newer giantmagnetostrictive materials have much higher coupling coefficients of more than $k = 0.70$ which makes it possible to operate the transducer at low Q and attain high power output simultaneously. For example, a Terfenol-D Tonpilz transducer similar to that depicted in Fig. 14a can produce a bandwidth of 200 Hz at a resonance frequency of 2 kHz ($Q = 10$) and a source level of 200 dB ref. 1 μPa at 1 m (35). Another Terfenol-D transducer reportedly produces a maximum output of 206 dB

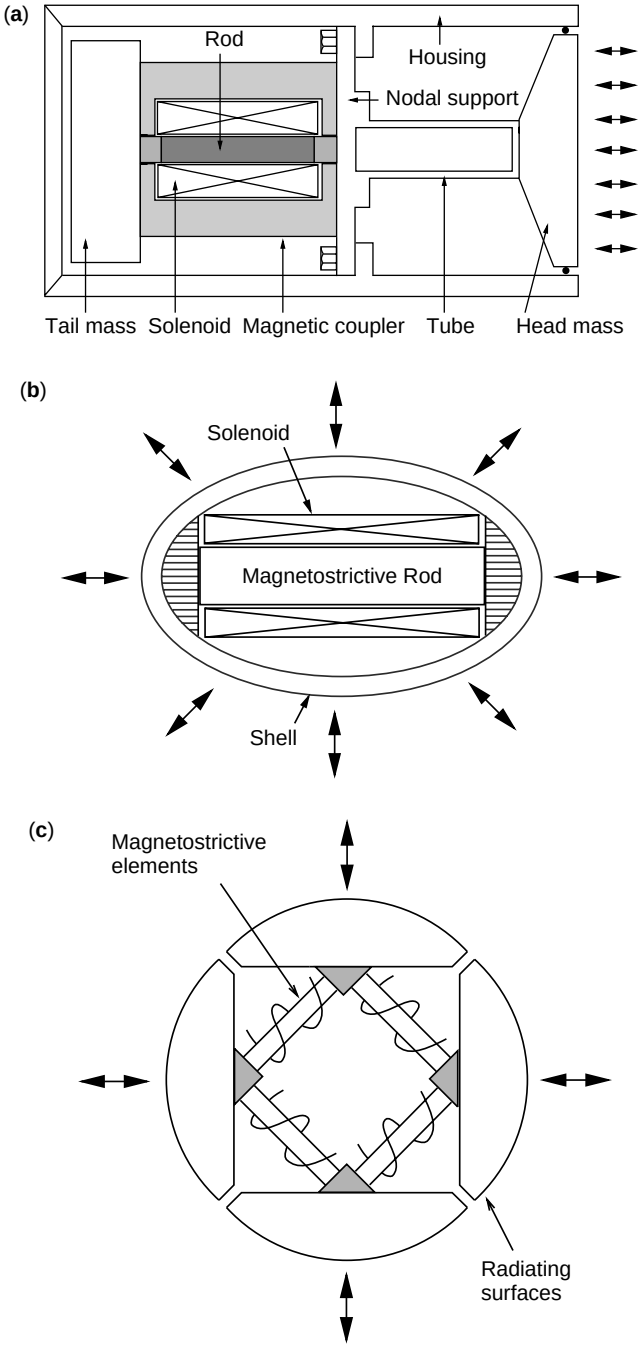

Figure 14. Magnetostrictive sonar transducers: (a) Tonpilz, (b) flextensional, and (c) square ring.

ref. 1 μPa at 1 m and operates across a broad usable bandwidth of 5–50 kHz (36). Other designs employ the linear motion of cylindrical magnetostrictive rods to flex a surrounding shell or to induce radial vibrations in a tube or ring, as shown in Fig. 14b,c. Further details and references are provided in (37).

Linear motors. Direct coupling between the load and the magnetostrictive element in Fig. 12 implies that the net load displacement is limited by magnetostriction. For instance, an 11.4-cm Terfenol-D actuator provides maximum displacements of about 0.2 mm. This displacement level is sufficient for many vibration control applications, but certain applications such as flow control valves or aircraft flap positioners typically require much larger strokes.

The fact that Joule magnetostriction takes place at constant volume is employed in the Kiesewetter motor to displace loads beyond the maximum strain normally achievable by a Terfenol-D rod. This motor (38) consists of a cylindrical Terfenol-D rod that fits snugly inside a stiff stator tube when no magnetic field is applied. Several short coils surround the stator to produce a magnetic field profile that sweeps along the Terfenol-D rod. When one of the coils is energized, for instance, coil 1 in Fig. 15a, the section of rod directly exposed to the magnetic field elongates and shrinks. As the field is removed, the rod clamps itself again inside the stator but at a distance d to the left of the original position. As the remaining coils are energized sequentially and the magnetic field profile is swept, the rod moves in a direction opposite to the sweeping field. The direction of motion is changed by inverting the sequence in which the coils are energized. From a design perspective, the total displacement is limited only by the length of the Terfenol-D rod, whereas the speed of motion is proportional to the sweeping frequency and the magnetostriction of the rod. Other factors that affect the smoothness and speed of the motor are the number of traveling pulses, the spacing between excitatory coils, the stiffness of the Terfenol-D material, and skin effect degradation due to eddy currents. The Kiesewetter motor is self-locking when unpowered, which is an important attribute for many robotic applications.

A proof-of-concept Kiesewetter motor presented in (39) produces 1000 N of force and 200 mm of useful stroke at a speed of 20 mm/s; it is intended for uses such as control of coat weight and fiber distribution in the paper industry and valve operation and precision positioners for the machine tool industry. An improved design presented in (40) addresses some of the technical problems of the Kiesewetter motor, particularly the degradation of fit between the stator and the rod caused by wear and thermal expansion. Furthermore, this revised design enables rotary motion in a way that is otherwise impossible to achieve by using the original Kiesewetter design.

Another variant of the inchworm principle is shown in Fig. 15b. This motor consists of translating clamps, fixed clamps, pusher transducers, and a load shaft. By coordinating the clamping and unclamping actions of the clamps with the action of the pushing transducers, it is possible to induce bidirectional motion of the load shaft. The load rating is limited by the frictional force between the clamps and the load shaft. Note that the inchworm principle can also be implemented by using other smart materials such as piezoelectric stacks (41) or a combination of piezoelectric and magnetostrictive elements, as shown later.

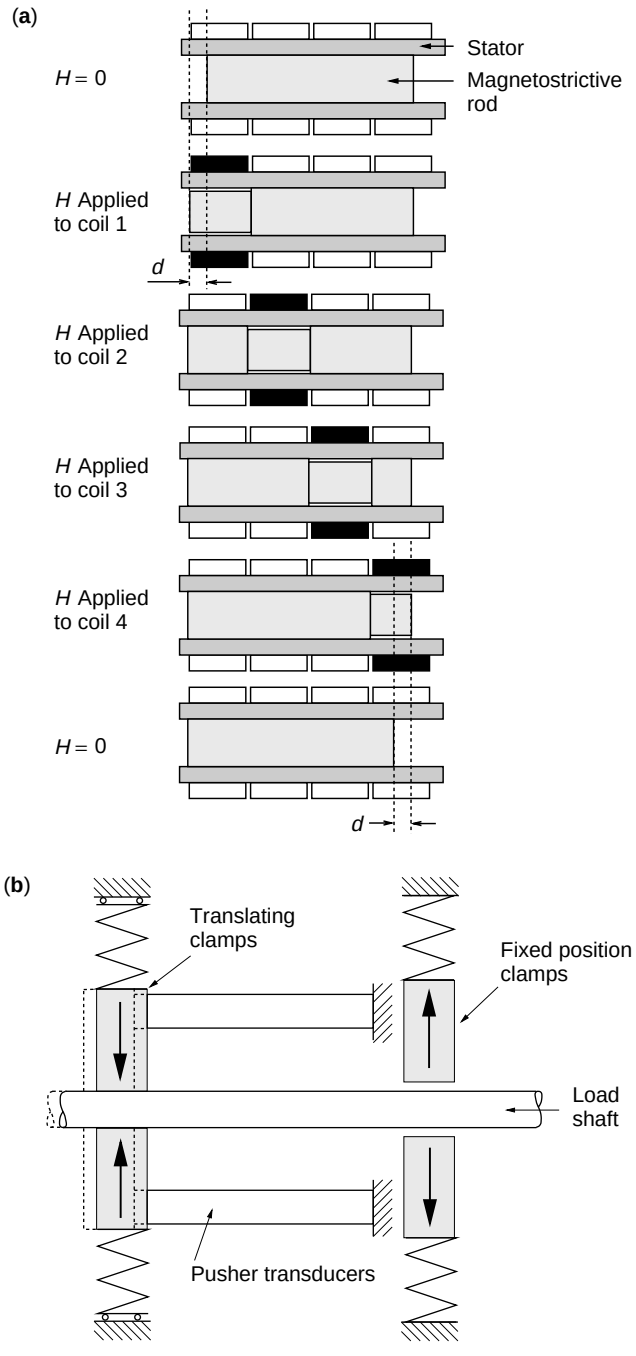

Figure 15. (a) The Kiesewetter inchworm motor. Black rectangles indicate energized coils; white rectangles indicate inactive coils. (b) Inchworm linear motor.

Piezoelectric transducers are often preferred for ultrasonic power generation in the megahertz range, but certain applications in the low-ultrasonic range benefit from the ruggedness and lack of depoling mechanisms of magnetostrictive materials. For instance, nickel is extensively used in applications such as degassing liquids (20–50 kHz)

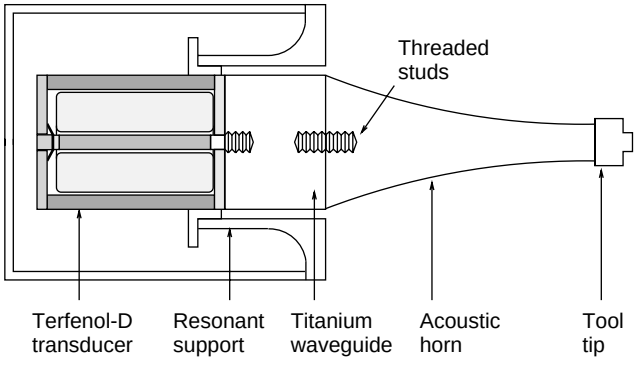

Figure 16. Schematic diagram of an ultrasonic Terfenol-D device consisting of a quarter-wave transducer coupled to a quarter-wave titanium waveguide and a half-wave acoustic horn. Different tool tips can be used as needed.

and cleaning dental or jewelry pieces (more than 50 kHz). A surgical ultrasonic tool based on Terfenol-D was developed recently that reportedly provides enhanced power and displacement output compared to existing piezoelectric tools; it is also lighter, more compact, and can deliver a 600-V, 1-MHz signal to cauterize bleeds without affecting its surgical function. In this device, illustrated in Fig. 16, a laminated quarter-wavelength Terfenol-D rod is coupled to a quarter-wavelength titanium waveguide that provides the resonant subassembly to which a half-wavelength acoustic horn is attached. The acoustic horn has an amplification factor from 15–30; thus, it provides extreme accelerations and energy concentration at the tip of the tool (42,43). Other current or potential uses for this transducer design include industrial cleaning, sonic cell disruption and sterilization, friction welding, and treatment of diverse chemical and biological processes (1).

Rotational Motors. Smart material motors based on the magnetostrictive principle are potentially simpler and more reliable than conventional hydraulic or electromagnetic systems. The inchworm technique has been employed in a rotational motor that produces a torque of 3 Nm at a speed of 0.5 rpm (44). Another inchworm type device also provides a speed of 0.5 rpm but produces a very high torque of 12 Nm and precision microsteps of 800 μrad (45). Despite the great positional accuracy and high holding torques, the current inchworm-type rotational motors tend to lack efficiency. Much of the efficiency limitation has been overcome in the resonant rotational motor proposed by Claeyssen et al. (46). Two linear Terfenol-D actuators are used to induce elliptical vibrations in a circular ring that acts as a stator and transmits the vibrations to rotational rotors pressed against the ring. The prototype reportedly provides a maximum torque of 2 Nm at a maximum speed of 17 rpm.

The field of ultrasonic rotational motors has aroused much research and commercial interest. These motors are employed in a wide range of applications from autofocusing camera lenses to robotic manipulators. A rotational actuator developed by Akuta (44) employs Terfenol-D to achieve a relatively high speed of 13.1 rpm and a maximum torque

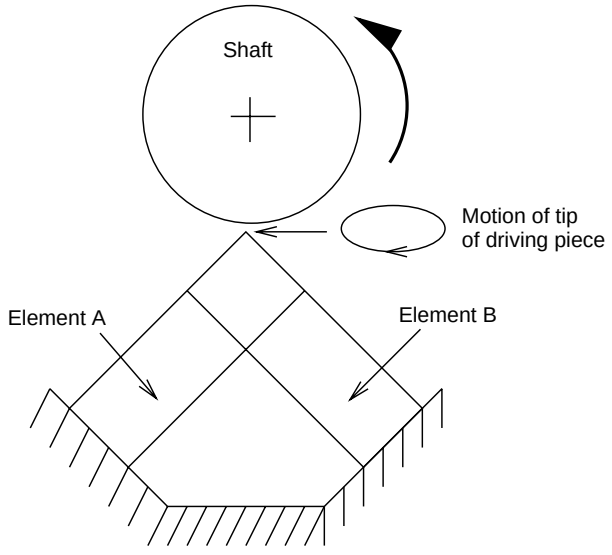

Figure 17. Rotational ultrasonic motor (44).

of 0.29 Nm. As depicted in Fig. 17, this motor employs two Terfenol-D exciter rods to induce rotations in the shaft.

Hybrid Magnetostrictive/Piezoelectric Devices. Given their technological interest, hybrid smart material actuators can be considered a separate class independently of whether they are intended for sonar, linear, or rotational applications. Because magnetostrictive materials are inductive and piezoelectric elements are capacitive, it is advantageous to combine both types of materials in the same device, so that a resonant electric circuit is formed. When driven at resonance, such a device behaves like a purely resistive load and only the energy that is effectively converted to mechanical motion or lost to inner losses needs to be supplied externally. This greatly simplifies amplifier design and helps to attain high efficiencies.

The hybrid device has been demonstrated that overcomes the difficulties involved in achieving motion at only one end of a Tonpilz piston-type sonar transducer; it consists of a quarter-wavelength stack of piezoelectric Navy type I ceramic rings joined to a quarter-wavelength Terfenol-D composite tube [see Fig. 18a and (47)]. The inherent 90° phase shift between the magnetostrictive and piezoelectric velocities in combination with the quarter-wavelength design of the elements ensures addition at one end and cancellation at the other. The device is *mechanically* unidirectional, but it becomes *acoustically* unidirectional only under array-baffled operation. The measured front-to-back pressure ratio is 5 dB for the device alone and 15 dB under array-loaded conditions. The concept of hybrid piezoelectric/magnetostrictive transduction has also been implemented for linear inchworm motors (48,49) and rotational motors (50). For example, the prototype presented in (48) has the configuration shown in Fig. 15b, but the clamping is done by piezoelectric stacks, and the translation is provided by Terfenol-D rods. The intrinsic 90° phase lag between the two types of elements provides natural drive timing for the inchworm, and the direction of motion

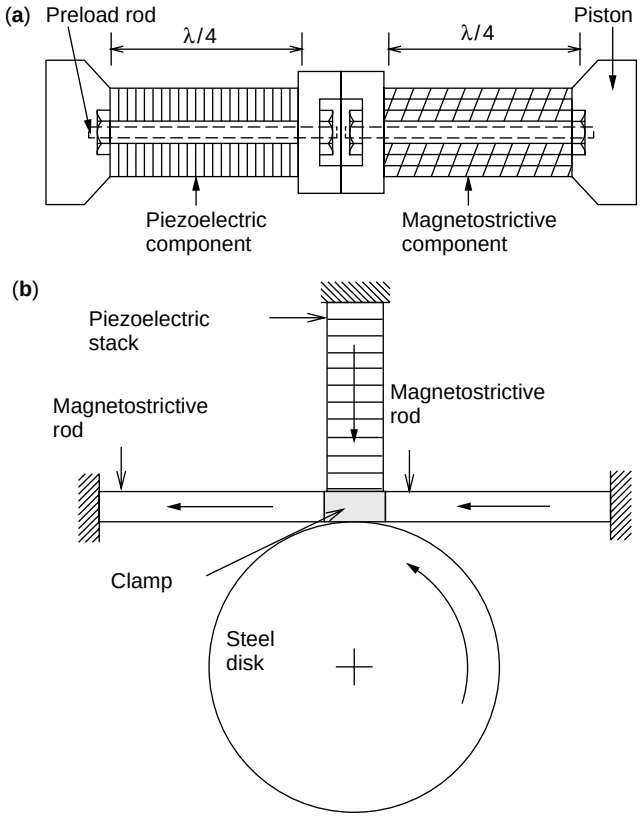

Figure 18. Hybrid magnetostrictive/piezoelectric transducers: (a) sonar projector (47); (b) rotational motor (50).

is easily reversed by changing the magnetic bias on the Terfenol-D elements. This motor achieves a zero-load speed of 25.4 mm/s and a stall load of 115 N.

The hybrid magnetostrictive/piezoelectric rotational motor illustrated in Fig. 18b follows the proof-of-concept transducer presented in (50). A piezoelectric stack clamps a piece of friction material onto the rotating disk, and two magnetostrictive rods move the clamp tangentially to the disk to produce rotational motion. As indicated before, the sequence of the motion is determined by the natural timing of the piezoelectric and magnetostrictive responses. The device produces a speed of 4 rpm at excitatory voltages from 30–40 V and frequencies from 650–750 Hz.

Sensor applications

Magnetostrictive materials are being employed in a wide variety of sensor designs as evidenced by the growing number of publications and patents. In this overview, the term sensor is used in a broad sense to indicate the attributes of magnetostrictive materials that facilitate generation of electrical signals in response to mechanical excitations, such as force, strain, and torque, or magnetic excitations such as magnetic fields. By virtue of the magnetomechanical coupling, changes in the magnetoelastic state through these parameters (or a combination of them) produce measurable change in magnetization anisotropy. To complete the sensing mechanism, a pick-up coil is often wrapped around the magnetostrictive material to detect magnetization changes; this effectively provides a mechanism for conversion of energy from magnetic to electrical regimes. The principle that links the magnetization with the voltage V generated across a pick-up coil is the Faraday–Lenz law of electromagnetic induction:

$$V = -NA\frac{dB}{dt},$$

in which N and A are, respectively, the number of turns and constant cross-sectional area of the coil and B is the magnetic induction that quantifies the magnetization state through the relationship $B = \mu_0(H + M)$ (21). Alternatively, interferometric techniques can be employed to detect the changes in wave speed that occur when the magnetostrictive material changes its properties in the presence of external excitations, for instance, the stiffness changes associated with the ΔE effect described earlier.

An overview of sensor designs is presented next. The main principles that enable operation of the sensors are emphasized. The list is not comprehensive, but it shows that a huge number of alternative designs can be devised based on the fundamental operation principles presented here. Further details can be found in the references provided.

Torque sensors. Magnetostrictive noncontact torque meters have been devised based on the principle that the torque applied to a shaft generates stresses of opposite sign, $+\tau$ and $-\tau$, oriented $\pm 45^\circ$ from the shaft axis. If the shaft is magnetostrictive or has a magnetostrictive amorphous ribbon bonded to it, the magnetic properties along the directions of $+\tau$ and $-\tau$ change as discussed previously. These properties can be measured either differentially by a set of perpendicular coils, as shown in Fig. 19a, or through a single Hall effect or similar magnetic field intensity sensor (51). This kind of sensor can be employed, for instance, in fly-by-wire steering systems for the automotive and aerospace industries. Additional details and references can be found in (2).

Another class of noncontact torque meters relies on the changes in permeability exhibited by a magnetostrictive material subjected to torsional stress. In particular, applications that require less sensitivity can benefit from the elevated mechanical strength that magnetic steels or alloys provide. One example is shown in Fig. 19b, where the working torque on a drill bit is detected by two sensing coils connected in series, one located over the flutes and the other over the shank (the permeability of the shank is less sensitive to changes in torque than the flutes.) A coil provides the ac magnetic field excitation, and the sensor's proportional output is the differential voltage generated by the sensing coils as the permeability of the bit changes due to the applied torque (52).

Deformational and Position Sensors. Transverse-field annealed magnetostrictive ribbons or wires make very sensitive strain gauges. A sensor of this kind has been made from strips of Metglas 2605SC transverse annealed for 10 min in a 208 kA/m (2.6 kOe) magnetic field at 390°C

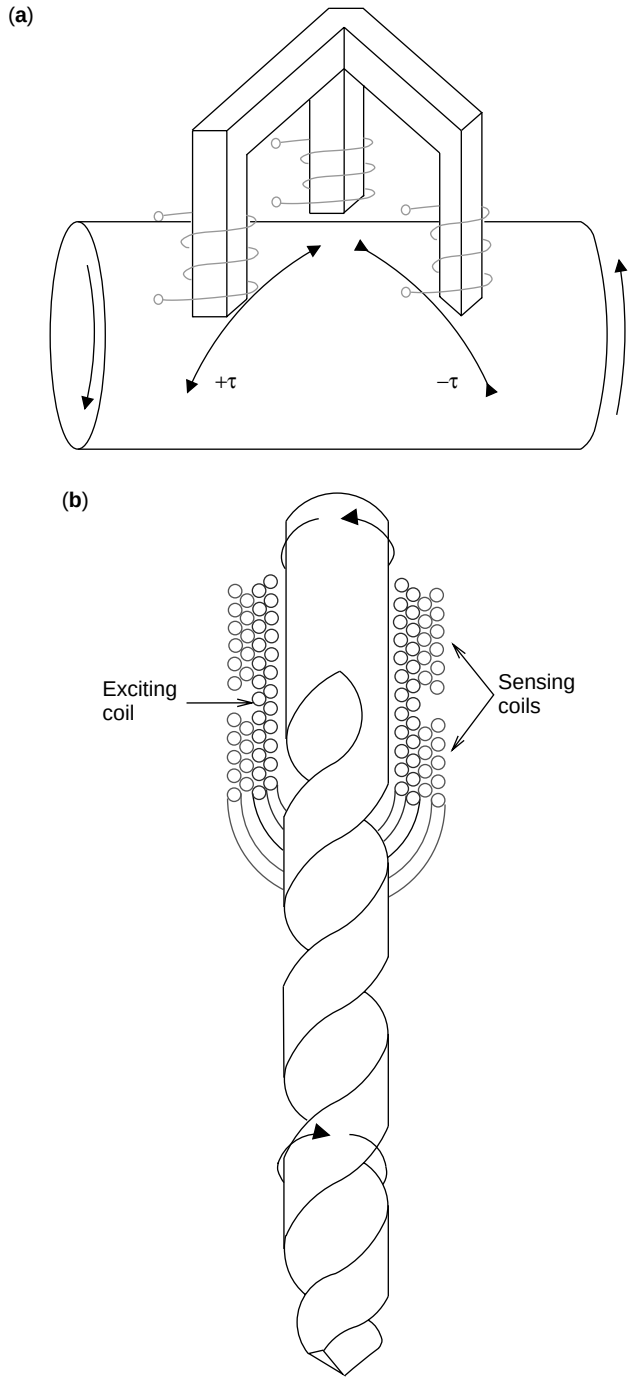

Figure 19. Magnetostrictive noncontact torque sensors: (a) Differential reading in directions oriented $\pm 45^{\circ}$ from the shaft axis and (b) differential reading of the permeability changes experienced by a drill bit subjected to a torque.

and rapidly cooled in a saturation field (53). The sensor responds to the changes in the permeability of the ribbon, which by virtue of the magnetomechanical coupling depends in turn on the state of strain in the material. Defining a dimensionless gauge factor as the fractional change in the measured parameter (in this case permeability) divided by the change in strain, $F = (\partial\mu/\partial S)/\mu$,

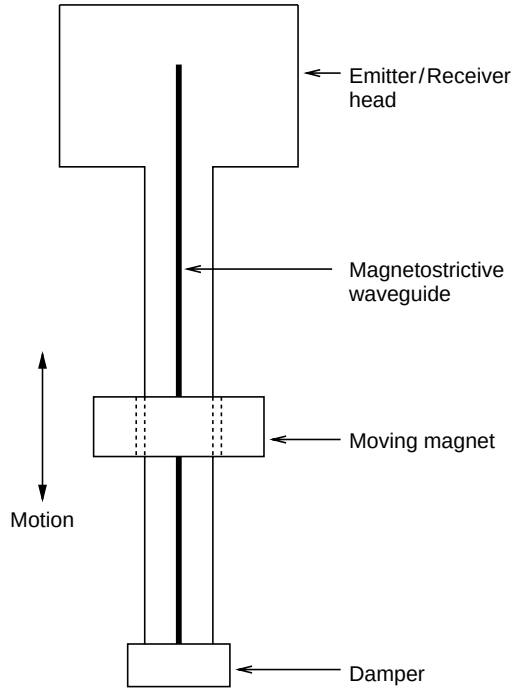

Figure 20. Magnetostrictive waveguide position sensor.

this sensor has an F value equal to about 250,000, which compares extraordinarily well with resistive strain gauges ($F = 2$) and semiconductor gauges ($F = 250$). One problem encountered in using this device is that normal thermal expansion can saturate the sensor. This problem can be overcome by bonding the material using a highly viscous liquid, although this limits operation to ac regimes.

A position detector can be made by using a magnetostrictive material as an acoustic waveguide. This device, shown in Fig. 20, consists of a permanent magnet that is connected to the target and rides along the length of the waveguide, an emitter/receiver head that sends and receives either an acoustic or current pulse down the waveguide, and a damper that prevents unwanted wave reflections. The sensor's operating principle is rather simple; the magnet interacts with the magnetostrictive waveguide and locally changes its material properties. These material property changes can be detected in different ways. In one version, the stiffness discontinuity produced by the magnet (ΔE effect, see earlier) partially reflects an acoustic pulse sent by the emitter. In a second version, the emitter sends a continuous current pulse down the waveguide that produces a circumferential magnetic field that interacts with the axial field from the magnet. The resulting helical field produces a twist in the wire (Wiedemann effect) that travels back to the receiver head. In both versions, the transit times of the original and reflected pulses provide a measure of the location of the magnet along the waveguide. This sensor can be used for measuring fluid levels by connecting the magnet to a float or for generic position sensing of up to 50 m at ± 1 mm accuracy (2).

Magnetometers. If the magnetostriction of a given material is known as a function of magnetic field, the problem

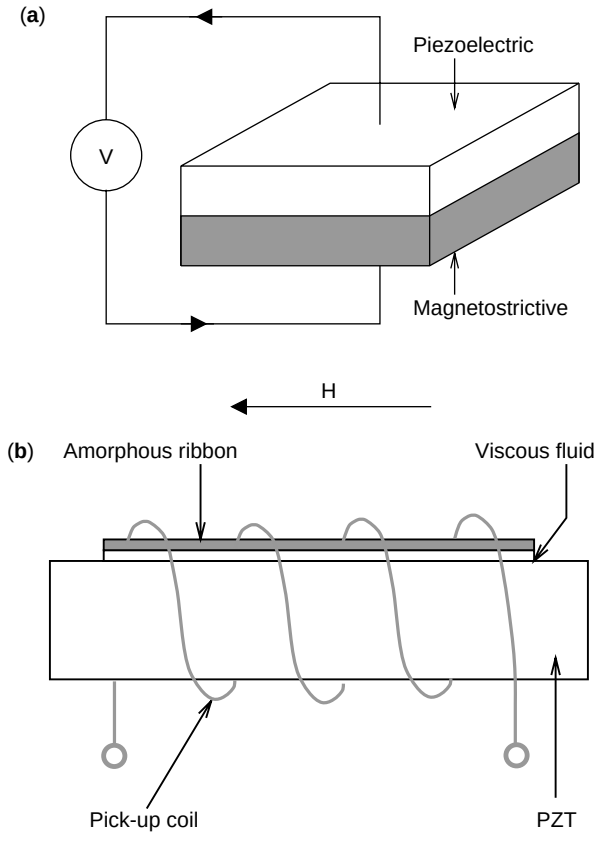

Figure 21. Hybrid magnetostrictive/piezoelectric magnetic field sensors. When a magnetic field is applied to one of these sensors, the magnetostrictive material strains, which either (a) generates a voltage across the piezoelectric plate or (b) induces an emf in a surrounding pick-up coil that can be extracted from the alternating carrier emf produced as the piezoelectric plate resonates.

of measuring the magnetic field reduces to one of measuring length. The length can be measured by a laser interferometer, optic fiber, strain gauge, capacitor, or another calibrated material such as a piezoelectric compound. For example, a very simple design consists of two slabs of magnetostrictive and piezoelectric materials bonded together (Fig. 21a). When a magnetic field is applied to the magnetostrictive material, it strains and induces a proportional voltage in the piezoelectric material. In another version, shown in Fig. 21b, a magnetometer is realized by bonding a field-annealed metallic glass ribbon onto a resonating PZT plate by using a viscous fluid. An alternating voltage is applied to the PZT plate, which generates a longitudinal stress field. By using proper bonding techniques, the dynamic stress in the metallic ribbon is congruent with that in the PZT, and the static component is filtered out by the viscous fluid. By virtue of the Villari effect, these dynamic stresses create an oscillating electromotive force (emf) in the surrounding pick-up coil. When exposed to low-frequency magnetic fields, a low-frequency emf is generated in the coil that is extracted from the carrier emf by conventional phase sensitive detection techniques. The measured detection limit can reach 6.9×10^{-6} A/m at 1 Hz (54), which compares with that of fluxgate magnetometers.

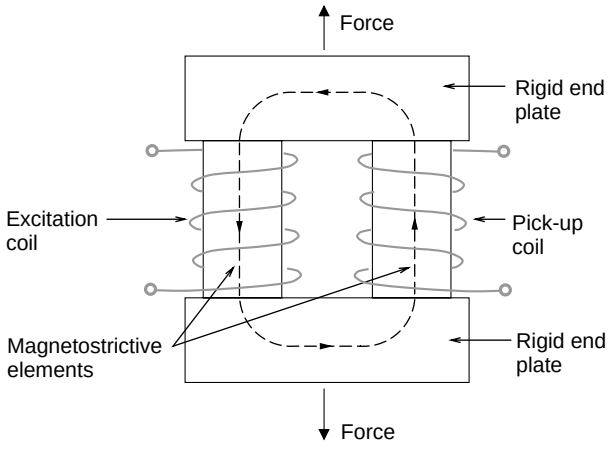

Figure 22. Magnetostrictive force sensor based on the Villari effect.

Another type of magnetometer consists of a magnetostrictive film bonded to an optic fiber. When the sensor is exposed to magnetic fields, the magnetostrictive material deforms and induces a deformation in the optic fiber. This causes changes in the optical path length of laser beams that pass through the optic fiber and can be detected by an interferometer (55). Highly sensitive metallic glass ribbons have been employed in devices so designed that yield quasistatic resolutions from 1.6×10^{-3}–8.0×10^{-3} A/m (56). Finally, a diode laser interferometer has been used to detect changes in the length of a Terfenol-D rod that are produced when a magnetic field is applied (57). A maximum sensitivity of 160×10^{-6} A/m was achieved, although certain nonlinear dependences were observed that make it critical to operate the sensor within its optimum mechanical preload range.

Force Sensors. By employing the Villari effect, it is possible to realize a simple and rugged force sensor from either crystal or amorphous magnetostrictive materials. The magnetostrictive attribute that provides the operating principle for such a sensor is the dependence of magnetization on the state of stress in a material. To illustrate, the design in Fig. 22 consists of two magnetostrictive elements, one surrounded by an excitation coil and the other surrounded by a pick-up coil, and two rigid end plates. In one mode of operation, an ac voltage is applied to the excitation coil that generates a magnetic flux in the sensor and a corresponding voltage in the sensing coil. As a force is applied, the magnetostriction in the elements produces a change in the magnetic flux that is detected as a proportional voltage change in the pick-up coil. In a second mode of operation at constant flux, the excitation voltage is allowed to change to maintain a constant pick-up coil output voltage. The change in excitation voltage is then related to the change in the applied force. Compared to conventional force sensors such as those based on strain gauges, this sensor is simpler, more rugged, and requires simpler electronics. A similar Villari effect sensor based on amorphous ribbons has been discussed in (58). Numerous other designs have been discussed or patented, including

percussion sensors, pressure sensors, and force sensors based on magnetoelastic strain gauges. The reader is directed to (2) for further details and references.

Transducer Models

Fundamental models of the performance of magnetostrictive materials used in smart structure systems are particularly difficult to develop. The difficulty lies in the coupling between regimes and the strong nonlinear dependence of material behavior on operating conditions and the hysteresis inherent in the materials. Notwithstanding, models based on physical principles are necessary to optimize transducer design and control, particularly considering that first-principles models provide the ability to *scale the results* in a sense that empirical models typically do not. These include magnetization models based on Preisach, Stoner–Wohlfarth, Jiles–Atherton, and micromagnetic theories, as well as domain rotation and higher order magnetostrictive models. However, comprehensive models for designing and controlling integrated smart structure systems must address the interaction between the magnetostrictive material's elastic, magnetic, thermal, and electrical regimes and the dynamics of the underlying structure. This can include elastic dynamics and also acoustics attributes. Following is an overview of models that have been employed to design and control magnetostrictive transducers. The reader is directed to the references for more comprehensive details on individual modeling techniques.

Piezomagnetic Constitutive Equations. Piezomagnetic models analogous to those classically employed for piezoceramics can prove useful for low drive level applications where hysteresis is minimal and behaviors are quasilinear. Neglecting thermal effects, the total strain ε of a magnetostrictive material includes two contributions: (1) the magnetostriction λ produced by the rotation of magnetic moments as they align with externally applied magnetic fields and (2) a purely elastic component $\varepsilon = s\,\sigma$ of the kind found in conventional nonmagnetic materials. Analogously, the magnetic induction B consists of two contributions: (1) a magnetomechanical component dependent on the stress and (2) the constant-stress magnetic constitutive law $B = \mu H$. From these considerations, the constitutive linearized equations that describe magnetostriction or piezomagnetism can be written in differential form, as follows:

$$\begin{aligned} \Delta\varepsilon &= s^H \Delta\sigma + d\,\Delta H, \\ \Delta B &= d^* \Delta\sigma + \mu^\sigma \Delta H, \end{aligned} \tag{9}$$

where ε is the total strain in the magnetostrictive material, s^H is the compliance at constant field H, d and d^* are the piezomagnetic coefficients, σ is the stress, B is the magnetic induction, and μ^σ is the magnetic permeability at constant stress.

The ratio of fundamental constants $k^2 = d^2/(s^H \mu^\sigma)$ for this one-dimensional linearized case provides a formulation which has been of value in describing the magnetomechanical coupling coefficient k of magnetostrictive materials. This coupling coefficient provides a measure of the conversion efficiency between magnetic and mechanical energies. Specifically, the magnetomechanical coupling coefficient squared represents the fraction of maximum stored magnetic energy that can be converted into elastic energy or conversely, the fraction of maximum stored elastic energy that can be converted into magnetic energy. It has been shown (59) that k can be expressed in terms of suitable internal energies,

$$k = \frac{U_{\mathrm{me}}}{\sqrt{U_{\mathrm{e}}\,U_{\mathrm{m}}}},$$

in which $U_{\mathrm{me}} = (1/2)\,H\,d^*\,\sigma$ is the magnetic energy due to elastic energy, $U_{\mathrm{e}} = (1/2)\,s\,\sigma^2$ is the elastic internal energy and $U_{\mathrm{m}} = (1/2)\,\mu\,H^2$ is the magnetic internal energy. Note that these expressions for k are based on the intrinsic assumption of piezomagnetic reciprocity, that is, $d = d^*$ and $U_{\mathrm{me}} = U_{\mathrm{em}} = (1/2)\,d\,H\,\sigma$. In that sense, these expressions must be employed strictly within the linear operating regimes in which the reciprocity assumption is sufficiently accurate. Typical values of the coupling constant are provided in Table 1. Further details can be found in (1,8).

The piezomagnetic model given by Eq. (9) has been augmented by adding saturation phenomena, temperature dependences, and the quadratic relationship between the magnetization and free strains given by Eq. (8). This higher order anhysteretic model has been described elsewhere (4). Like the original formulation from which it derives, this augmented model has the advantage of simplicity in addition to adding certain nonlinear features. In this model, however, complete nonlinear phenomena or hysteretic effects can be addressed only by using complex model parameters. Furthermore, this model addresses material attributes primarily but disregards important transducer effects such as the electrical and dynamic regimes. These effects have been addressed to some degree by coupling the piezomagnetic equations (9) with transducer models such as the linearized canonical equations for electromechanical transducers,

$$\begin{aligned} V &= Z_{\mathrm{e}}\,I + T_{\mathrm{em}}\,v, \\ F &= T_{\mathrm{me}}\,I + z_{\mathrm{m}}\,v, \end{aligned} \tag{10}$$

that describe the behavior of a "black box" analog of a transducer system that consists of two coupled electrical and mechanical regimes (60,61). In these equations and Fig. 23,

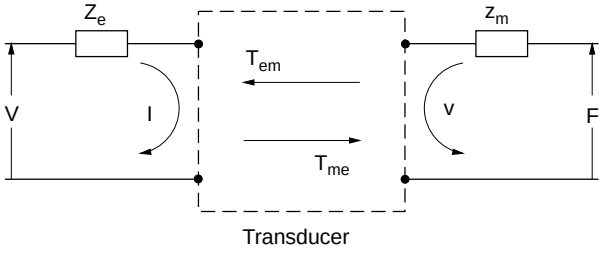

Figure 23. Schematic representation of an electromechanical transducer.

V and I are the voltage and current in the coil, Z_e is the blocked electrical impedance (electrical impedance that is observed when the mechanical system is prevented from moving), F and v are force and velocity on the mechanical side, z_m is the mechanical impedance, and T_{em} and T_{me} represent transduction coefficients that describe the electromechanical coupling. Although this model is phenomenological, certain loss mechanisms based on physical effects such as eddy currents have also been incorporated (1).

Magnetization Models. Magnetization plays a fundamental role in both the magnetostriction that arises from the rotation of magnetic moments (actuator mode) and the change in magnetic anisotropy that occurs when the material strains (sensor mode). From a modeling perspective, the hysteretic phenomena that arise as magnetic moments rotate in response to magnetic fields, stresses, or thermal energy are often the primary magnetization attribute that needs to be quantified. Models for magnetization hysteresis in ferromagnetic materials range from micromechanical models to phenomenological characterizations. Micromechanical models (28,62) describe the coupled magnetoelastic interactions through first-principles formulations that involve the elasticity, thermodynamics, and the electromagnetic energy states. This can lead to highly accurate results at the magnetic domain level, but the large number of parameters required currently prohibits implementing micromechanical models at the system level. The Preisach model has been extensively used to characterize the magnetization of ferromagnetic materials, and more recently of magnetostrictive materials as well (63–66). This model approximates the multivalued hysteretic map by employing a parallel collection of operators. This method has the advantage of intrinsic generality, but typically it requires identifying a large number of nonphysical parameters, and it does not employ or provide insights regarding the dynamics of the system. One advantage of this method is that the Preisach operator can be inverted to facilitate linear control design. Domain rotation models include the classical anisotropic formulation of Stoner and Wohlfarth (18) and later extensions to include cubic anisotropies (67) and compressive loading effects (19). A more complete generalization includes anisotropy, magnetoelastic, and field energies in all three spatial directions (20). Although model results agree well with measured data, identifying the fractional occupancies that define the participation of different easy axes in the total magnetization is rather complex. The domain wall theory of Jiles and Atherton has provided accurate results in ferromagnetic (68), magnetostrictive (30,69), and ferroelectric (70–72) materials. This model is constructed from a thermodynamic difference between the magnetic energy available to magnetize a material and the energy lost as domain walls attach to and detach from inclusions or pinning sites in the material. This yields a set of differential equations that depend on five physical parameters which quantify reversible, irreversible, and total magnetization changes. In the limit when domain wall pinning goes to zero, the Jiles–Atherton model reduces to Langevin's anhysteretic function, although alternative anhysteretic models that employ the Isin spin relation have been studied (72). Finally, the Jiles–Atherton model has been employed in combination with Eq. (8) to map the H–λ constitutive relationship (24), and later with dynamical transducer effects to provide a set of reciprocal constitutive relationships among H, M, ε, and σ (30,69). This modeling approach has proven useful in inverse compensation designs (73), characterization of collocated actuation and sensing in transducers (74), and quantification of the ΔE effect in magnetostrictive materials (75).

CONCLUDING REMARKS

Magnetostrictive materials are a class of smart materials that can convert energy between the magnetic and elastic states. The phenomenon of magnetostriction is ultimately due to the coupling between magnetic moment orientation and interatomic spacing, or magnetomechanical coupling. This type of coupling provides a mechanism for bidirectional conversion of energy between magnetic and elastic regimes which is attractive for actuator and sensor systems because it does not degrade in time and it provides almost immediate response. Newer materials such as Terfenol-D or amorphous metallic ribbons exhibit a unique combination of high forces, strains, energy densities, operating bandwidths, and coupling coefficients that justify their use in an ever-increasing number of applications ranging from micropositioners to vibration control systems for heavy machinery. The excellent performance of magnetostrictive materials is sometimes obscured by the large magnetic hysteresis losses and substantial nonlinear effects exhibited by these materials when operated at the high regimes in which their attributes become more prominent. In this sense, realizing the full potential of magnetostrictive materials presents rigorous engineering challenges in a way that other less capable smart materials do not. However, as evidenced by the increasing number of patented devices based on magnetostrictive principles, designers continue to overcome these challenges and make advances in designing, modeling, and controlling magnetostrictive transducers. Furthermore, clever transducer designs are possible solely due to the rich performance space that arises from the otherwise undesirable nonlinear characteristics of these materials. As material advances continue, it is expected that magnetostrictive device designers will find new magnetostrictive solutions for an ever-growing variety of transducer applications.

BIBLIOGRAPHY

1. G. Engdahl ed., *Handbook of Giant Magnetostrictive Materials*. Academic Press, San Diego, 2000.
2. E. du Trémolet de Lacheisserie, *Magnetostriction Theory and Applications of Magnetoelasticity*. CRC, Boca Raton, FL, 1993.
3. T. Cedell, Ph.D. thesis, Lund University, Lund, Sweden, 1995. LUTMDN/(TMMV-1021)/1-222/(1995).
4. T.A. Duenas, L. Hsu and G.P. Carman, in *Advances in Smart Materials Fundamentals and Applications*. Boston, 1996.

5. M. Anjanappa and Y. Wu, *Smart Mater. Struct.* **6**:393–402 (1997).
6. H. Uchida, M. Wada, A. Ichikawa, Y. Matsumara, and H.H. Uchida, *Proc. Actuator 96, 5th Int. Conf. New Actuators*, Bremen, Germany, 1996, pp. 275–278.
7. C. Body, G. Reyne, and G. Meunier, *IEEE Trans. Magn.* **33**(2):1620–1623 (1997).
8. A. E. Clark, in *Ferromagnetic Materials*, E.P. Wohlfarth, ed., North Holland, Amsterdam, 1980, Vol. 1, Chap. 7, pp. 531–589.
9. E.A. Lindgren, J.C. Poret, J.J Whalen, L.P. Martin, M. Rosen, M. Wun-Fogle, J.B. Restorff, A.E. Clark, and J.F. Lindberg, *U.S. Navy Workshop Acoust. Transduction Mater. Devices*, State College, PA, April 13–15, 1999.
10. J.B. Restorff, M. Wun-Fogle, and A.E. Clark, *U.S. Navy Workshop Acoust, Transduction Mater. Devices*, State College, PA, April 13–15, 1999.
11. R. Tickle, R.D. James, T. Shield, M. Wuttig, and V.V. Kokorin, *IEEE Trans. Magn.* **35**(5):4301–4310 (1999).
12. R.C. O'Handley, *J. Appl. Phys.* **83**(6):3263–3270 (1998).
13. B.D. Cullity, *Introduction to Magnetic Materials*, Addison-Wesley, Reading, MA, 1972.
14. R.M. Bozorth, *Ferromagnetism*. Van Nostrand, New York, 1968.
15. C. Kittel, *Rev. Mod. Phys.* **21**:541–583 (1949).
16. E.W. Lee. *Rep. Prog. Phys.* **18**:184–220 (1955).
17. J.P. Teter, A.E. Clark, and O.D. McMasters, *J. Appl. Phys.* **61**:3787–3789 (1987).
18. E.C. Stoner and E.P. Wohlfarth, *Philos. Trans. R. Soc.* **A240**:599–642 (1948).
19. A.E. Clark, H.T. Savage, and M.L. Spano, *IEEE Trans. Magn.* **MAG-20**(5): pp. 1443–1445 (1984).
20. D.C. Jiles and J.B. Thoelke, *J. Magn. Magn. Mater.* **134**:143–160 (1994).
21. D.C. Jiles, *Introduction to Magnetism and Magnetic Materials*. 2e, Chapman & Hall, London, 1998.
22. S. Chikazumi, *Physics of Magnetism*. Krieger, Malabar, FL, 1984.
23. M.J. Dapino, A.B. Flatau, and F.T. Calkins, *Proc. SPIE Smart Struct. Mater. 1997*, San Diego, March 1997, Vol. **3041**, pp. 256–267.
24. F.T. Calkins, R.C. Smith, and A.B. Flatau, *IEEE Trans. Magn.* **36**(2):429–439 (2000).
25. D.C. Jiles, *J. Phys. D Appl. Phys.* **28**:1537–1546 (1995).
26. M.J. Sablik and D.C. Jiles, *J. Appl. Phys.* **64**(10):5402–5404 (1988).
27. M.J. Sablik and D.C. Jiles, *IEEE Trans. Magn.* **29**(4): pp. 2113–2123 (1993).
28. R.D. James and D. Kinderlehrer, *Philos. Mag. B* **68**(2):237–274 (1993).
29. V. Agayan, *Physica Scripta* **54**:514–521 (1996).
30. M.J. Dapino, R.C. Smith, L.E. Faidley, and A.B. Flatau, *J. Intelligent Mater. Syst. Struct.* 11(2): 135–152 (2000).
31. A.B. Flatau, M.J. Dapino, and F.T. Calkins, *Proc. SPIE Smart Struct. Mater.* San Diego, March 1998, Vol. **3327**, pp. 463–473.
32. F.T. Calkins and A.B. Flatau, *Proc. SPIE Smart Struct. Mater. 1996*, San Diego, March 1996, Vol. **2717**, pp. 709–719.
33. A.B. Flatau, F. Pascual, M.J. Dapino, and F.T. Calkins, CATD-IPIRT Contract #95-05, October 1996.
34. F.T. Calkins, M.J. Dapino, and A.B. Flatau, *Proc. SPIE Smart Struct. Mater. 1997*, San Diego, CA, Vol. **3041**, pp. 293–304.
35. G.A. Steel, in *Transducers for Sonics and Ultrasonics*, Technomic, Lancaster, PA, 1993, pp. 250–258.
36. J.B. Restorff, in *Encyclopedia of Applied Physics*, VCH, New York, 1994, Vol. **9**, pp. 229–244.
37. M.J. Dapino, F.T. Calkins, and A.B. Flatau, in *22nd Encyclopedia of Electrical and Electronics Engineering*, J.G. Webster, ed., Wiley, NY, 1999, Vol. **12**, pp. 278–305.
38. L. Kiesewetter, *Proc. 2nd. Int. Conf. Giant Magnetostrictive Alloys*, Marbella, Spain, October 12–14, 1988.
39. R.C. Roth, *Proc. 3rd Int. Conf. New Actuators*, Bremen, Germany, 1992, pp. 138–141.
40. J.H. Goldie, M.J. Gerver, J. Kiley, and J.R. Swenbeck, *Proc. SPIE Smart Struct. Mater. 1998*, San Diego, March 1998, Vol. **3329**, pp. 780–785.
41. W. Chen, J. Frank, G.H. Koopmann, and G.A. Lesieutre, *Proc. SPIE Smart Struct. Mater. 1999*, Newport Beach, CA, March 1999.
42. T.T. Hansen, Technical report, Chemtech, American Chemical Society, 1996, pp. 56–59.
43. J.R. Frederick, *Ultrasonic Engineering*. Wiley, NY, 1965.
44. T. Akuta, *Proc. 3rd. Int. Conf. New Actuators*, Bremen, Germany, 1992, pp. 244–248.
45. J.M. Vranish, D.P. Naik, J.B. Restorff, and J.P. Teter, *IEEE Trans. Magn.* **27**:5355–5357 (1991).
46. F. Claeyssen, N. Lhermet, and R.L. Letty, *IEEE Trans. Magn.* **32**(5):4749–4751 (1996).
47. J.L. Butler, S.C. Butler, and A.L. Butler, *J. Acoust. Soc. Am.* **94**:636–641 (1993).
48. J.E. Miesner and J.P. Teter, *Proc. SPIE Smart Struct. Mater. 1994*, Orlando, FL, 1994, Vol. **2190**, pp. 520–527.
49. B. Clephas and H. Janocha, *Proc. SPIE Smart Struct. Mater. 1997*, San Diego, March 1997, Vol. **3041**, pp. 316–327.
50. R. Venkataraman, W.P. Dayawansa, and P.S. Krishnaprasad, Technical report, CDCSS, University of Maryland, College Park, MD, 1998.
51. I.J. Garshelis, *IEEE Trans. Magn.* **28**(5):2202–2204 (1992).
52. I. Sasada, N. Suzuki, T. Sasaoka, and K. Toda, *IEEE Trans. Magn.* **30**(6):4632–4635 (1994).
53. M. Wun-Fogle, H.T. Savage, and M.L. Spano, *J. Mater. Eng.* **11**(1):103–107 (1989).
54. M.D. Mermelstein and A. Dandridge, *Appl. Phys. Lett.* **51**(7):545–547 (1987).
55. A. Yariv and H. Windsor, *Opt. Lett.* **5**:87 (1980).
56. A. Dandridge, K.P. Koo, F. Bucjolts, and A.B. Tveten, *IEEE Trans. Magn.* **MAG-22**:141 (1986).
57. R. Chung, R. Weber, and D.C. Jiles, *IEEE Trans. Magn.* **27**(6):5358–5360 (1991).
58. J. Seekercher and B. Hoffmann, *Sensors and Actuators* **A 21–A 23**:401–405 (1990).
59. D.A. Berlincourt, D.R. Curran, and H. Jaffe, in *Physical Acoustics, Principles and Methods*, W.P. Mason ed., Academic Press, NY, 1964, Vol. **1**, Part A.
60. F.V. Hunt, *Electroacoustics: The Analysis of Transduction and Its Historical Background*. American Institute of Physics for the Acoustical Society of America, 1982.
61. D.L. Hall, Ph.D. Dissertation, Iowa State University, Ames, Iowa, 1994.
62. W.F. Brown, *Magnetoelastic Interactions*. Springer-Verlag, Berlin, 1966.
63. I.D. Mayergoyz, *Mathematical Models of Hysteresis*. Springer-Verlag, NY, 1991.

64. J.B. Restorff, H.T. Savage, A.E. Clark, and M.Wun-Fogle, *J. Appl. Phys.* **67**(9):5016–5018 (1990).
65. A. Reimers and E. Della Torre, *IEEE Trans. Magn.* **35**:1239–1242 (1999).
66. R.C. Smith, *J. Math. Syst. Estimation Control* **8**(2):249–252 (1998).
67. E.W. Lee and J.E. Bishop, *Proc. Phys. Soc.* London **89**:661 (1966).
68. D.C. Jiles and D.L. Atherton, *J. Magn. Magn. Mater.* **61**:48–60 (1986).
69. M.J. Dapino, R.C. Smith, and A.B. Flatau, *IEEE Trans. Magn.* **36**(3):545–556 (2000).
70. R.C. Smith and C.L. Hom, *J. Intelligent Mater. Syst. Struct.* **10**(3):195–213 (1999).
71. R.C. Smith and Z. Ounaies, *J. Intelligent Mater. Syst. Struct.* **11**(1):62–79 (2000).
72. R.C. Smith, Smart structures: model development and control applications. Technical Report CRSC-TR01-01, Dept. of Mathematics, North Carolina State Univ., Raleigh, NC, 2001.
73. R.C. Smith and R.L. Zrostlik, *Proc. 1999 IEEE Conf. Decision and Control*, Phoenix, AZ, December 7–10, 1999.
74. M.J. Dapino, F.T. Calkins, R.C. Smith, and A.B. Flatau, *Proc. ACTIVE 99*, Ft. Lauderdale, FL, December 2–4, 1999, Vol. **2**, pp. 1193–1204.
75. R.C. Smith, M.J. Dapino, and A.B. Flatau, *Proc. SPIE Smart Struct. Mater. 2000*, Newport Beach, CA, March 6–9, 2000, Vol. **3985**, pp. 174–185.
76. D.C. Jiles, *Introduction to the Electronic Properties of Materials*. Chapman & Hall, London, 1994.
77. R.A. Kellogg and A.B. Flatau, *Proc. SPIE Smart Struct. Mater. 1999*, Newport Beach, CA, March 1999, Vol. **3668**.
78. A.E. Clark, J.P. Teter, M. Wun-Fogle, M. Moffett, and J. Lindberg, *J. Appl. Phys.* **67**(9): pp. 5007–5009 (1990).
79. F.T. Calkins, Ph.D. Dissertation, Iowa State University, Ames, Iowa, 1997.

MICROROBOTICS, MICRODEVICES BASED ON SHAPE-MEMORY ALLOYS

YVES BELLOUARD
Institut de Systèmes Robotiques
Ecole Polytechnique Fédérale de Lausanne
Switzerland

INTRODUCTION

For the past few years, consumer products such as computers, mobile phones, and cameras have drastically decreased in size and their functionalities have increased. In addition, mini-invasive techniques in surgery have led to a growing need for small, highly reliable components that can go through arteries or veins. In general, there are nearly no highly technological products that do not benefit from miniaturization. However, one cannot simply scale down electrical or mechanical components from "macroscale" because physical forces do not scale down at the same amplitude. Therefore, the efficiency of actuators depends on their size. Consequently, there is a need for new actuating technologies adapted to the microworld that can replace usual actuators such as electromagnetic motors. Among these technologies, smart materials such as piezoceramics, magnetostrictive, electrostrictive, and shape-memory materials are of particular interest. This article describes the use of shape-memory alloys (SMA) for microengineering applications.

In the first part, a brief description of SMA properties is given. The second part addresses some usual design principles. Finally, a literature survey and a concept of monolithic microdevices concludes the article.

SHAPE-MEMORY ALLOYS (SMA): A SUMMARY OF THEIR PROPERTIES

Properties of SMA: A Brief Description

Three main functionalities can be associated with the martensitic transformation: the shape-memory effect, superelasticity, and high damping capability. Special care is taken to describe the shape-memory effect, which is the essence of the SMA actuator. For a thorough understanding, the reader may refer to other sections of this encyclopedia. General books about SMA material may also be consulted (1–3).

The shape-memory effect. This happens when a material, previously deformed in martensite—the low-temperature phase—recovers its original shape when heated up to the austenite—the high-temperature phase. Figure 1 illustrates the shape-memory effect. The graph on the left side represents the stability zone for the two phases in a stress–temperature representation. According to the Clausius–Clapeyron relationship between stress and temperature, the oblique lines indicate the boundary between phases and the transition period. The martensitic transformation occurs across a given range of temperature (M_s to M_f, from austenite to martensite and A_s to A_f, from martensite to austenite).

Let us consider an example: a strip that is flat in the austenite phase, that is, the "memorized shape" (step 1 in Fig. 1). If a stress is applied below the martensite finish temperature (M_f) and if this stress is higher than the critical stress to detwin martensite, the variant reorientation occurs, and the strip is deformed in a plasticlike way (step 2). This means that when the stress is released, almost all of the deformation remains. When the material is heated above A_f (step 3), the material transforms to austenite and recovers its original shape. Repetitive cooling (step 4) does not cause any shape change.

The term "one-way, shape-memory-effect" is often used to address this effect, because it is a one-time occurrence; the material keeps its original austenitic shape upon further cooling cycles below M_f. Because nonoriented martensite is created upon cooling, martensitic structures have the same specific macroscopic volume as the austenitic crystal. A plasticlike deformation of martensite ("detwinning") is required to observe a shape change while heating up to the austenite. This phenomenon can be well understood using a one-dimensional phenomenological model